Atmospheric Environment 318 (2024) 120246

Contents lists available at ScienceDirect

Atmospheric Environment

journal homepage: www.elsevier.com/locate/atmosenv

Factors governing the chemical composition of rain at a regional site in South Africa

L. Kok [a], P.G. van Zyl [b,*], J.P. Beukes [b], R.P. Burger [a], S.M. Ellis [c], M. Josipovic [b], K. Jaars [b], V. Vakkari [b,d], L. Laakso [b,d], M. Kulmala [e]

[a] Unit for Environmental Sciences and Management, North-West University, Potchefstroom, South Africa
[b] Atmospheric Chemistry Research Group, Chemical Resource Beneficiation, North-West University, Potchefstroom, South Africa
[c] Statistical Consultation Services, North-West University, Potchefstroom, South Africa
[d] Finnish Meteorological Institute, Atmospheric Composition Unit, Helsinki, Finland
[e] Institute for Atmospheric and Earth System Research, University of Helsinki, Helsinki, 00014, Finland

HIGHLIGHTS

- Statistical analyses revealed correlations between rain chemistry and air mass history, and highlighted the complexity.
- Higher concentrations of ionic species were associated with air masses at 100 m a.g.l. passing over anthropogenic sources.
- No significant correlations between air mass histories at cloud base height and ionic composition were evident.
- Below-cloud atmospheric chemical composition was more significant to rain chemistry in this part of South Africa.
- Case studies signified the influence of several factors on rain chemistry.

ARTICLE INFO

Keywords:
Rain chemistry
Wet deposition
Cloud base height
Air mass history
Welgegund

ABSTRACT

Precipitation chemistry is influenced by a number of complex processes, which include the temporal and spatial evolution of air masses. Previous wet deposition studies in South Africa could not distinctly relate the influence of air mass history on rain chemistry in order to substantiate the influence of different sources. The Welgegund atmospheric monitoring station in South Africa measures several atmospheric parameters, which include vertical profiling of the atmosphere that could assist in relating rain chemistry to air mass history. Therefore, the aim of this study was to conduct an advanced assessment on factors influencing chemical composition of rain in the South African interior by relating individual rain events at Welgegund to air mass history at cloud base height (CBH) and arrival heights below clouds, as well as supplementary *in situ* measurements conducted at the site. Hierarchical cluster analysis was performed through two approaches, i.e. clustering based on the chemical composition of rain, as well as grouping based on air masses arriving at CBH and 100 m above ground level (a.g.l.). Although statistical analyses highlighted the complexity associated with correlating rain chemistry to sources of chemical species, it proved useful to determine some correlations between rain chemistry and air mass history. Clustering according to the chemical composition of rain events grouped rain events from high to low volume weighted mean (VWM) concentrations. Correlation of air mass histories to these clusters indicated that higher VWM concentrations were associated with air masses at 100 m a.g.l. passing over anthropogenic source regions. Air mass history clustering grouped air masses passing predominantly over predefined source regions. The rain chemistry of clusters determined for air masses at 100 m a.g.l. arrival heights could be related to the influence of different source regions, with the impact of large point sources, the clean western background region and oceans especially evident. No significant correlations between air mass histories at CBH and ionic composition were evident. It was concluded that below-cloud atmospheric chemical composition was more significant to the chemical composition of rain in this part of South Africa. A few case studies were also conducted in order to further explore factors influencing the chemical composition of rain.

* Corresponding author.
E-mail addresses: lizekok64@gmail.com (L. Kok), pieter.vanzyl@nwu.ac.za (P.G. van Zyl), Beukes@steinert.com.au (J.P. Beukes), Roelof.Burger@nwu.ac.za (R.P. Burger), Suria.Ellis@nwu.ac.za (S.M. Ellis), Micky.Josipovic@nwu.ac.za (M. Josipovic), Kerneels.Jaars@nwu.ac.za (K. Jaars), Ville.Vakkari@fmi.fi (V. Vakkari), Lauri.Laakso@fmi.fi (L. Laakso), markku.kulmala@helsinki.fi (M. Kulmala).

https://doi.org/10.1016/j.atmosenv.2023.120246
Received 4 July 2023; Received in revised form 16 November 2023; Accepted 22 November 2023
Available online 27 November 2023

1. Introduction

Precipitation chemistry reflects the major physical and chemical mechanisms in the atmosphere, while it also corresponds to changes in atmospheric chemical composition associated with anthropogenic activities and changes in meteorological patterns (Galy-Lacaux et al., 2009; Laouali et al., 2012; Schwab et al., 2016). Precipitation chemistry is influenced by a number of complex processes occurring in the water cycle between the surface of the earth and the atmosphere (Hall, 2003; Pauliquevis et al., 2012), as well as the temporal and spatial evolution of air masses (Fedkin et al., 2019; Lutgens and Tarbuck, 1982; Uchiyama et al., 2019). These processes include cloud nucleation, microphysical droplet interactions, cloud mechanics and precipitation, as well as emissions, chemical reactions and transport of species (Al-Khashman, 2009; Zhang et al., 2012).

Water-soluble chemical compounds can be introduced into droplets during cloud formation and lifetime, or during the precipitation event. Typical cloud condensation nuclei (CCN) include dust, sea salt, sulphate (SO_4^{2-}) and organic species (Christner et al., 2008; Feltracco et al., 2019; Uchiyama et al., 2019; Wallace and Hobbs, 2006). These species can either be primarily emitted from local sources or can be formed as secondary particulates in the atmosphere, which can be associated with long-range transport of air masses (Orué et al., 2019; Seinfeld and Pandis, 2006; Wallace and Hobbs, 2006). After a cloud is formed, in-cloud mixing occurs between different droplets, while various aqueous reactions take place that can be catalysed by species in interstitial cloud air (Brimblecombe, 2003; Hall, 2003; Pauliquevis et al., 2012). The inclusion of particulates or gaseous species into a cloud or droplet is referred to as scavenging. In-cloud scavenging entails the absorption of species into the droplet during droplet formation and/or from the interstitial atmosphere, while typical below-cloud scavenging processes include collision-coalescence, sweep-out, wake-capture, and diffusio- and thermophoresis. Scavenging efficiency depends on numerous factors, which include terminal velocity of the raindrops, collision efficiency, diffusivity, raindrop and particle size distributions, the electric field and polarisation, and rain intensity. Smaller droplets, for instance, will scavenge more efficiently due to slower terminal velocities and larger mass transfer coefficients (Hall, 2003; Lutgens and Tarbuck, 1982; Pauliquevis et al., 2012; Preston-Whyte and Tyson, 1988; Xu et al., 2017), while higher scavenging ratios are also associated with larger particles and increased rain intensity (González and Aristizábal, 2012; Kulshrestha et al., 2009).

The South African interior holds numerous large anthropogenic point sources of sulphur (S) and nitrogen (N), which include 12 coal-fired power plants, petrochemical industries and pyrometallurgical smelters (Lourens et al., 2012; Meth, 2018; Stern, 2006). In addition, domestic burning and open biomass burning are also important sources of atmospheric pollutants (Chiloane et al., 2017; Yao et al., 2015). A recent study by Conradie et al. (2016) reported wet deposition composition at four regionally representative background sites in the north-eastern interior of South Africa from 2009 to 2014, which was also compared to previous wet deposition studies in this region (Mphepya et al., 2004, 2006). An increase in the total ionic concentration and corresponding wet deposition fluxes was observed, which was attributed to increased anthropogenic activities and population growth. Kok et al. (2021) also assessed rain chemistry and wet deposition fluxes at Welgegund, which is a regional background atmospheric monitoring station impacted by the major source regions in the interior of South Africa (Jaars et al., 2016; Venter et al., 2017). At all these sites, which included two rural background sites, it was shown that SO_4^{2-} dominated rain chemistry, while relatively high contributions were also determined for nitrate (NO_3^-) and ammonium (NH_4^+). In addition, the average pH of rain at all these sites were well below the natural value, signifying the influence of anthropogenic activities on rainwater chemical composition in the South African interior (Conradie et al., 2016; Kok et al., 2021). Mompati et al. (2022) also quantified wet deposition at four sites from the far northern savanna through to the fynbos of the southern coast of South Africa, which also indicated high levels of S and N deposition.

In these above-mentioned wet deposition studies different source groups influencing the chemical composition of rain were determined with statistical and empirical methods. Back trajectories could not be effectively utilised to determine the influence of air mass history on individual rain events due to logistical constraints. In addition, since these sites were remote, they were equipped with basic instrumentation required for deposition studies. However, *in situ* measurements of numerous atmospheric parameters are conducted at Welgegund (Beukes et al., 2015), which allows advanced assessment of precipitation chemistry. Specific measurements that could assist in interpreting the chemical composition of rain samples include vertical profiling of the atmosphere and a rain intensity meter. Vertical profiles can be utilised to determine cloud base height (CBH) during the onset of a rain event, which can be associated with air mass history in order to evaluate the influence of source regions on specific rain events (Sun et al., 2010; Xu et al., 2017). Other ancillary measurements at Welgegund, such as gaseous and particulate measurements, could also assist in understanding the chemical composition of rain. Therefore, the aim of this study was to conduct an advanced assessment on factors influencing chemical composition of rain in the South African interior by relating individual rain events at Welgegund to air mass history at CBH and arrival heights below clouds, as well as supplementary *in situ* measurements conducted at the site.

2. Experimental

2.1. Sampling site

Rain samples were collected at the Welgegund atmospheric measurement station (26°34′10″S, 26°56′21″E), which is a regional background site located on a commercial farm approximately 100 km west from the Johannesburg-Pretoria megacity (Fig. 1). There are no large point sources within proximity of Welgegund, but it is impacted by air masses passing over the major source regions in the interior of South Africa (Kok et al., 2021), which include the Johannesburg-Pretoria conurbation, the western Bushveld complex (pyrometallurgical smelters and mines), the Mpumalanga Highveld (nine coal-fired power stations and petrochemical plant) and the Vaal Triangle (petrochemical plant, coal-fired power station, pyrometallurgical smelters). In addition, Welgegund is also impacted by a relatively clean region in the south-west to northern sector where no large point sources are located (Fig. 1), which include the Nama-Karoo biome (desert and xeric shrubland) that is a regional source of wind-blown dust (Venter et al., 2017, 2018). Detailed descriptions on the source regions impacting Welgegund and the regional meteorology, as well as the surrounding vegetation, soil and agricultural activities have been presented (e.g. Booyens et al., 2015; Jaars et al., 2016; Kok et al., 2021; Venter et al., 2017).

Welgegund experiences a typical subtropical climate (temperatures ranging from sub-zero during winter up to maximum temperatures well over 30 °C in summer), while it is also characterised by distinct wet and dry seasons typical of the South African Highveld. The dry season corresponds with the colder months from mid-May to mid-October, while the wet season coincides with warmer months from mid-spring to mid-autumn (Tyson and Preston-Whyte, 2017). More pronounced inversion layers occurring during winter also causes pollutant build-up in the atmosphere during these months, with these air masses being recirculated through the dominant high-pressure system over this region (Tosen and Jury, 1988; Tyson et al., 1976). Rainfall in this region is mainly convective, with convective rainfall events predominantly occurring during the afternoon or early evenings (Harrison, 1986; Hart et al., 2010; Tyson and Preston-Whyte, 2017). The annual average rainfall over subtropical southern Africa is approximately 500 mm (Harrison, 1986).

2.2. Measurements

2.2.1. Rain sampling and analyses

Detailed descriptions of the collection and chemical analysis of rain samples at Welgegund, as well as the quality control and -assurance procedures are presented by Kok et al. (2021) and Conradie et al. (2016). In short, rain sampling procedures, chemical analysis and data processing complied with the field protocols and data quality objectives (DQOs) for precipitation chemistry measurements of the World Meteorological Organisation (WMO and WATCH, 2004). A custom-made automated wet-only sampler (based on the *Aerochem Metrics* model 301) was used to collect event-based rain samples. Samples were collected immediately after a rain event, which was stored frozen until analysis. After thawing and filtering the rain samples, the pH and electrical conductivity (EC) (*Hanna Instruments* HI 255) was measured, whereafter samples were analysed with a Dionex ICS 3000 ion chromatograph (IC). Inorganic ionic species measured included SO_4^{2-}, NO_3^-, chloride (Cl^-), fluoride (F^-), NH_4^+, calcium (Ca^{2+}), potassium (K^+), magnesium (Mg^{2+}) and sodium (Na^+), while water-soluble organic acids (OAs), i.e. acetic- (CH_3COO^-), formic- ($HCOO^-$), oxalic- ($C_2O_4^{2-}$) and propionic acid ($C_3H_5O_2^-$) were also determined. Volume weighted mean (VWM) concentrations ($\mu eq.L^{-1}$) of these species were determined, while deposition fluxes were calculated by multiplying VWM concentrations with rainfall depth (Conradie et al., 2016; Kok et al., 2021).

Two tipping-bucket rain gauges, i.e. a *Vaisala* QMR102 and a *Casella* 0.1 mm were used to determine starting times of rain events, rain depth (mm) and rain intensity ($mm.h^{-1}$). Measurements from both instruments were combined in this study.

2.2.2. Cloud base height (CBH)

CBH was measured with a *Vaisala* CT25K ceilometer, which uses LIDAR (light detection and ranging) technology (Gierens et al., 2019). A short pulse laser is emitted and a returning signal is detected, from which the profile of the attenuated backscatter coefficient (β') can be retrieved (Emeis et al., 2012; Vaisala, 1999). The ceilometer has a 15 s temporal and 30 m vertical resolution up to 7.5 km in the atmosphere, which was averaged to 15 min and 210 m (Gierens et al., 2019). The instrument was also tilted four degrees from the vertical towards the south to avoid reflection from ice clouds.

Three respective CBH layers can be obtained from the backscatter values determined with the ceilometer. However, clouds can occur in more than three distinct layers or in merged layers, while different layers can also obscure each other (Costa-Surós et al., 2013). Therefore, in this study, an assumption was made to only consider the lowest CBH detected by the ceilometer. Other CBH layers were only detected in a few instances, which were not significantly higher than the lowest CBH. This can be attributed to merging of cloud layers or other layers being obscured by the lowest layer. An average CBH was calculated for the 2-h period prior to the onset of a rain event, which enabled calculation of three hourly-arriving back trajectories at CBH during the beginning of a rain event in order to reduce error margins associated with individual back trajectories, which will be explained later (Section 2.3).

2.2.3. Ancillary measurements

Ancillary measurements continuously performed at Welgegund were used to assist in elucidating factors influencing the chemical composition of rain. General meteorological parameters measured in addition to precipitation included temperature (T), relative humidity (RH), wind speed (WS) and -direction (WD), and atmospheric pressure (P). Atmospheric trace gas measurements included SO_2 (*Thermo-Electron* 43S SO_2 analyzer), NO_x (*Teledyne* 200AU NO_x analyser), O_3 (*Environment* SA41M O_3 analyser) and CO (*Horiba* APMA-360 CO analyzer). Particulate measurements included PM_{10} concentrations with a Synchronized Hybrid Ambient Real-time Particulate Monitor (*Thermo Scientific* Model 5030 SHARP), while equivalent black carbon (eBC) measurements were conducted with a Multi-Angle Absorption Photometer (*Thermo Scientific* Model 5012 MAAP).

In addition to ancillary measurements conducted at Welgegund, daily fire distribution data was derived from satellite retrievals of the National Aeronautics and Space Administration's (NASA) Moderate Resolution Imaging Spectrometer (MODIS) mounted on the polar-orbiting Earth Observation System's (EOS) Terra satellite. Burn scar data for 4 days prior to a rain event for the entire southern Africa was retrieved from the NASA Distributed Active Archive Centres (DAAC)

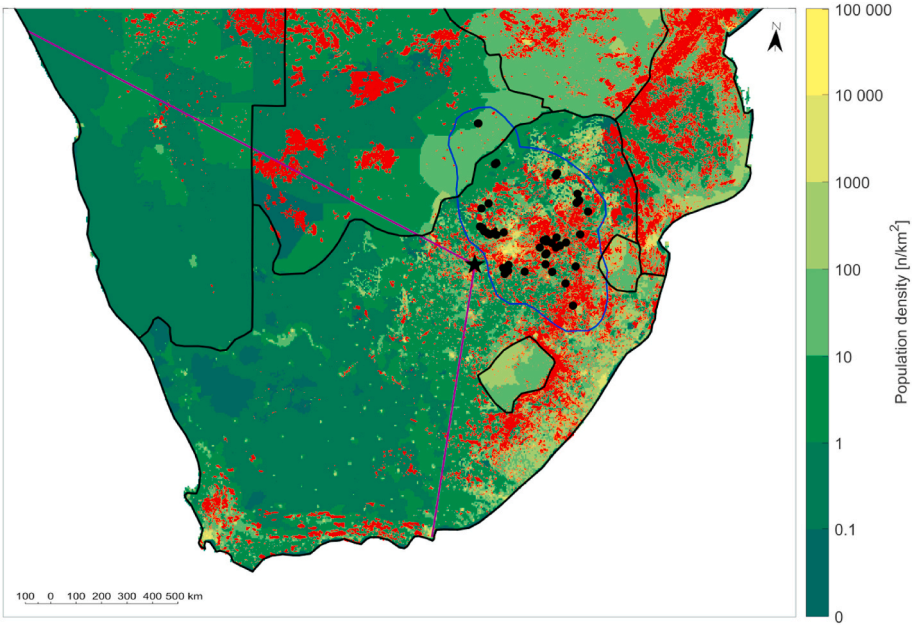

Fig. 1. A map of southern Africa indicating the 2010 population density estimate for South Africa (CIESIN, 2010), the MODIS burned areas (red areas) for 4 days prior to a rain event, major point sources (black dots) impacting Welgegund (black star), and the source regions defined in this study. The purple lines separate the source regions into the relatively clean north-west to south-western sector with no large point sources, and an eastern region that is densely populated, has extensive open biomass burning occurrences and includes major point sources in the South African interior. The blue polygon indicates the source region including only the major point sources and the JHB-PTA conurbation.

(Kaufman et al., 2003), which are presented in Fig. 1. The South African population density estimate for 2010 was obtained from the Centre for International Earth Science Information Network and are also indicated in Fig. 1 (CIESIN, 2010). Each rain event was also related to surface synoptic charts obtained from the South African Weather Service (SAWS) (SAWS, 2019) and infrared satellite images from the European Organisation for the Exploitation of Meteorological Satellites (EUMETSAT, 2019).

2.3. Relating rain events to air mass history

Back-trajectories were calculated using the National Oceanic and Atmospheric Administration (NOAA) Air Resource Laboratory's (ARL) Hybrid Single-Particle Lagrangian Integrated Trajectory (HYSPLIT) model (version 4.8) (Fleming et al., 2012; Stein et al., 2015), while meteorological input data for the model was retrieved from the Global Data Assimilation System (GDAS) archive of the US National Weather Service's National Centre for Environmental Prediction (NCEP). Three hourly-arriving 96-h back trajectories were calculated at two arrival heights i.e. 100 m and CBH for each rain event sampled. A back trajectory was calculated at the starting time of the rain event, with an additional two trajectories calculated one and 2 h prior to the onset of the rain event at the two heights indicated. This was done in order to reduce the 15–30% uncertainty associated with individual back trajectories (Stohl et al., 2002). Back trajectories associated with the 100 m a.g.l. arrival height were considered representative of air mass history related to below-cloud scavenging. Since orography is not well defined in the HYSPLIT model, arrival heights lower than 100 m a.g.l. increase the estimated error margins on individual trajectories (Stohl et al., 2002). The boundary layer was also considered to be well mixed during the wet season, which is supported by Gierens et al. (2019) who indicated rapid evolution of the boundary layer after sunrise.

The time that air masses arriving at 100 m a.g.l. and CBH spent over predefined source regions prior to arrival at Welgegund was determined. These source regions are presented in Fig. 1, which included an area to the west and a region to the east of Welgegund demarcated by the purple lines. The sector to the west represents the relatively clean background region with no large point sources. The eastern area includes the major point sources in the interior of South Africa, while this region is also densely populated with extensive biomass burning occurring in this sector (Fig. 1). This eastern area was further separated into two source regions. The first source region included the major point sources in the interior of South Africa, i.e. coal-fired power stations, pyrometallurgical smelters and petrochemical industries, as well as the JHB-PTA conurbation (indicated by the blue polygon in Fig. 1). The second source region excluded these large point sources, which represented the regional impacts associated with large point sources, household combustion and open biomass burning. The total time that air masses spent over oceans was also quantified.

2.4. Statistical analysis

The chemical composition of wet deposition (Kok et al., 2021), as well as air mass histories at CBH and 100 m a.g.l., were subjected to hierarchical cluster analysis (HCA) (*STATISTICA*, (StatSoft, 2006) and *SPSS Statistics*). Two approaches were followed, i.e. (1) clustering based on the chemical composition of rain and, (2) clustering according to air mass history at 100 m a.g.l. and CBH. The first approach determined clusters of strong correlations between ionic species in rainwater, which was then related to air mass history at CBH and 100 m a.g.l., as well as rain intensity and ancillary measurements. The second approach clustered the average time that back trajectories arriving at Welgegund at CBH and 100 m a.g.l. spent over different source regions (Fig. 1), which was then associated with ionic composition of rainwater, as well as rain intensity and ancillary measurements. The method of Ward was followed in which the squared Euclidean linkage distances were determined to reveal optimum cluster solutions, which also minimises the loss of information contained in each cluster. Since the ideal cluster solution is subjective and subject to some variability, the agglomerate schedule coefficients – a measure of heterogeneity between groups – were plotted, which revealed relatively ideal cluster solutions descriptive of the data within each group and are not too specific for a particular sample, i.e. meaningful solutions. The most significant decrease in the coefficient differences were considered optimum cluster solutions. Three clusters were determined to be optimum solutions for the each of the approaches followed in this study. Higher than three-cluster solutions resulted either in increased or negligible changes in heterogeneity.

An analysis of variance in cluster solutions was conducted by evaluating the statistical and substantive significance of different clusters, i.e. P-values <0.05 were regarded to be statistically significant, while effect sizes were also considered. Effect sizes enables a standardised metric regardless of scale, which allows comparisons and identification of relationships between quantities with different units and sizes (Ellis and Steyn, 2003). Furthermore, it limits the possible overestimation associated with only considering statistical significance. Cohen's d values were utilised in this study, which describe the standardised mean difference of the effect as presented in Equation (1) (Cohen, 1988; Ellis and Steyn, 2003; Lakens, 2013):

$$d = \frac{|\bar{x}_1 - \bar{x}_2|}{s_{max}} \quad (1)$$

where d = Cohen's effect size, $\bar{x}_1$ and $\bar{x}_2$ are the means of two samples being compared, and s_{max} is the maximum standard deviation of the two groups. Effect sizes are considered small for d = 0.2, medium for d = 0.5, and large for d = 0.8 (Cohen, 1988; Ellis and Steyn, 2003; Lakens, 2013). A large effect size implies considerable variances for a variable in different clusters, which is an important factor characterising different clusters. Effect sizes can also be used to determine the significance of overlap between different clusters, which were therefore also used in this study to relate clusters determined with the different approaches to each other.

3. Results and discussion

Only rain events for which collected samples passed the WMO DQO criteria were considered. In addition, rain events coinciding with gaps in ancillary data collected at Welgegund (e.g. due to power failures), as well as for which no back trajectories were available (e.g. due to gaps in the GDAS archive), were also excluded. In total, 86 rain events were considered. All three hourly-arriving 96-h air mass back trajectories calculated for Welgegund at 100 m a.g.l. and CBH for all rain event during the entire sampling period were overlaid, while the total time that air masses at both arrival heights spent over the predefined sources regions prior to the afore-mentioned rain events were also calculated (Figure A1). Air masses arriving at both arrival heights at Welgegund spent most time over the eastern sector. A larger fraction of air masses at an arrival height of 100 m a.g.l. passed over the source region wherein the large point sources are located compared to CBH air mass arrival heights, whereas more air masses arriving at CBH at Welgegund passed over the western background region. This is indicative of below-cloud scavenging possibly being an important factor contributing to chemical composition in rain samples collected at Welgegund, which will be further explored. Furthermore, air masses arriving at CBH spent relatively more time over oceanic regions compared to air masses at an arrival height of 100 m a.g.l.

3.1. Clustering chemical composition of rain

As mentioned above, clustering analysis based on ionic composition of rainwater revealed three significant clusters. In Table 1 the VWM concentrations of ionic species in each of these clusters are presented,

while pH, electrical conductivity (EC), rainfall depth and ancillary measurements at Welgegund associated with each cluster are also included. These clusters, i.e. CHEM-A, CHEM-B and CHEM-C represented 70, 25 and 5% of all rain samples, respectively.

It is evident from Table 1 that the optimum three clusters determined represent varying levels of VWM concentrations of ionic species, i.e. VWM concentrations of species in cluster CHEM-A were the lowest with the corresponding lowest total VWM concentration, while the VWM concentrations of ionic compounds in cluster CHEM-C were the highest (with the exception of H^+) with a resultant highest total VWM concentration. Furthermore, cluster CHEM-C also had the highest EC value. Cluster CHEM-A represented that largest number of rain events, while cluster CHEM-C comprised the lowest number of events. Cluster CHEM-B had higher H^+ levels (and lowest pH) compared to that of CHEM-C, which can be attributed to decreased neutralisation of acidic species by Ca^{2+} in this cluster. The ratios of Ca^{2+} levels compared to concentrations of other species in cluster CHEM-C were significantly higher compared to similar ratios in the other two clusters. The extent of neutralisation of acidic species through Ca^{2+} in rain samples collected at Welgegund was indicated by Kok et al. (2021). Cluster CHEM-A is associated with the highest rainfall depth, while cluster CHEM-C corresponds to the lowest rainfall depth. In Kok et al. (2021) and Conradie et al. (2016), the lower rainfall depths were associated with higher VWM concentrations at Welgegund and other sites in the interior of South Africa. Cluster analyses according to ionic composition of rainwater did not reveal any significant chemical compositional differences between clusters, with the exception of proportionally higher Ca^{2+} and Mg^{2+} concentrations in cluster CHEM-C compared to other species. The cluster analyses simply grouped rain events in relation to total VWM concentrations of ionic species from high to low.

Comparison of the ancillary measurements in each of the clusters indicated that the concentrations of most pollutant species (e.g. SO_2, CO, eBC, PM_{10}) were higher in CHEM-B and CHEM-C. Although it is difficult to directly quantify the influence of primary emitted species on rain chemistry, these measurements reflect the influence of the eastern pollution source regions on rain chemistry at Welgegund. In addition, higher PM_{10} concentrations could have a more direct influence on the chemical composition of rain. A more distinct correlation is observed between the VWM concentrations of ionic species and rain intensity in Table 1 with higher VWM concentrations associated with increased rain intensity. Cluster CHEM-C, with the higher VWM concentrations and the highest rainfall intensity, also corresponded to lower average CBH 15 min prior to a rain event, as well as to the greatest difference between the 2-h and 15-min CBH averages, and lowest RH. CHEM-A had the smallest difference in CBH averages, as well as the lowest rainfall intensity and the highest RH.

An analysis of variance on the levels of each of these ancillary measurements, as well as pH and EC in the three clusters was also conducted to establish statistical and substantive significance. The p-values and size effect (Cohen's d-value) for measurements for which significant differences between different clusters were calculated were considered (Table A1). The effect sizes indicate the effect of the variable on the distinction between events in different clusters. No meaningful statistical and substantive differences were determined EC, SO_2, and eBC when comparing cluster CHEM-B and CHEM-C, while pH and rain intensity differed significantly. Comparison of cluster CHEM-A with clusters CHEM-B and CHEM-C revealed meaningful differences between all the measurements considered (Table A1). The major ancillary factors not included in the cluster analysis that differed significantly between all three clusters were pH and rain intensity.

Table 1
VWM concentrations ($\mu eq.L^{-1}$) of ionic species in each cluster determined, as well as average pH, electrical conductivity (EC), total rainfall depth over the sampling period, average rainfall depth per rain event, as well as averages of ancillary measurements in a 2-h period before the rain event. The standard deviations are indicated in brackets.

	CHEM-A		CHEM-B		CHEM-C	
# of samples	68		24		5	
H^+	20.38	[23.35]	39.06	[25.51]	31.04	[23.35]
Na^+	11.48	[19.09]	22.69	[57.60]	47.37	[19.09]
NH_4^+	22.28	[16.60]	28.07	[22.74]	34.85	[16.60]
K^+	4.26	[6.87]	8.88	[22.91]	11.68	[6.87]
Mg^{2+}	4.79	[7.11]	5.92	[12.05]	76.60	[7.11]
Ca^{2+}	15.84	[17.15]	21.98	[35.57]	85.08	[17.15]
NO_3^-	24.91	[19.04]	33.54	[28.47]	58.24	[19.04]
Cl^-	11.71	[18.26]	24.16	[60.36]	39.38	[18.26]
SO_4^{2-}	33.8	[24.11]	57.59	[32.22]	86.41	[24.11]
F^-	0.30	[0.24]	0.87	[1.01]	0.84	[0.24]
tOA*	8.89	[13.38]	9.21	[22.50]	20.35	[13.38]
Total VWM	158.64		251.96		491.84	
pH	4.8	[0.52]	4.59	[1.94]	5.96	[1.94]
EC	25.04	[20.37]	55.81	[57.85]	59.64	[42.97]
SO_2 (ppb)	0.5	[0.68]	1.91	[3.64]	0.97	[0.81]
NO (ppb)	0.12	[0.29]	0.00	[0.20]	−0.01	[0.17]
NO_x (ppb)	2.72	[2.09]	3.15	[3.83]	1.91	[1.30]
O_3 (ppb)	32.17	[11.76]	34.38	[11.08]	34.58	[7.74]
CO (ppb)	123.39	[36.70]	129.00	[40.99]	145.92	[25.93]
eBC ($ug.m^{-3}$)	0.26	[0.27]	0.49	[0.68]	0.40	[0.27]
PM_{10} ($ug.m^{-3}$)	14.5	[11.79]	18.03	[9.49]	23.40	[12.17]
RH (%)	65.1	[21.70]	59.88	[20.08]	64.94	[19.00]
Average (max) rain intensity ($mm.h^{-1}$)	4.04 (12.27)	[3.10] [7.80]	5.27 (20.88)	[4.62] [19.00]	7.22 (43.36)	[4.22] [27.78]
Total (avg) rainfall (mm)	809.50 (11.9)	[9.40]	614.50 (25.60)	[18.90]	193.00 (38.6)	[23.54]
CBH 2hr (m)	2284.84	[1032.47]	2263.18	[735.43]	2394	[669.09]
CBH_15 min (m)	1961.72	[893.66]	1870.91	[751.40]	1412	[563.27]

In Figs. 2 and 3, air mass histories at 100 m a.g.l and CBH associated with each rain event in the three clusters determined through cluster analysis of the ionic composition of rain samples are presented. It is evident that air masses with a 100 m a.g.l. arrival height at Welgegund for rain events associated with cluster CHEM-B and CHEM-C spent similar periods over the source region containing the large point sources, while air masses determined for cluster CHEM-A spent relatively less time over this source region. All air masses arriving at 100 m a.g.l. spent similar times over the eastern source region excluding the large point sources, while a relatively higher percentage of these air masses passed over oceans for cluster CHEM-C. The main difference between air masses arriving at Welgegund at 100 m a.g.l. in the three clusters relates to the time spent over the clean western sector. Air masses with an arrival height of 100 m a.g.l. in cluster CHEM-C spent significantly more time over the western source region compared to cluster CHEM-B, and relatively more time than that of cluster CHEM-A. Therefore, this could explain the significantly higher Ca^{2+} and Mg^{2+} in cluster CHEM-C in relation to the other species. Kok et al. (2021) attributed the increased neutralisation of rainwater at Welgegund compared to other site in the South African interior to air masses passing over this background region west of Welgegund where areas such as the Karoo and Kalahari are located. No significant differences are observed for air masses arriving at CBH at Welgegund for the three clusters, with the exception of air masses arriving at CBH determined for cluster CHEM-C spending more time over the source region containing large point sources. Therefore, this could partially contribute to higher VWM concentrations of ionic species in the cluster.

Although air mass histories and ancillary measurements explain some variances between the clusters to a certain extent, the total rainfall depth associated with each of these clusters seems to be the major factor

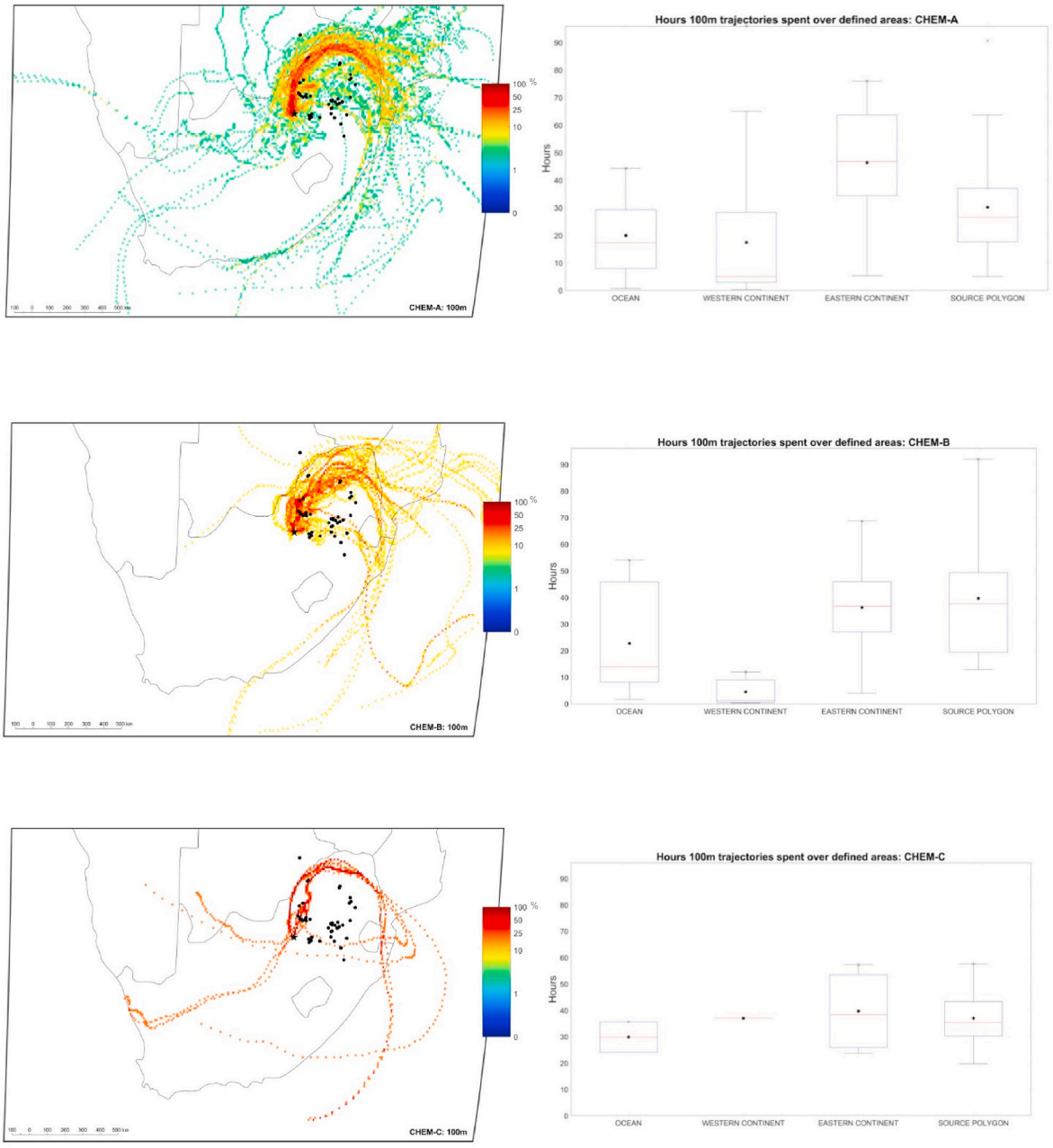

Fig. 2. 96-h overlay back trajectories for air masses arriving at 100m a.g.l. for each rain event in cluster CHEM-A, CHEM-B and CHEM-C at Welgegund. The colour scale bar presents the frequency (percentage) of air masses passing over a region. Boxplots presents the total time that air masses spent over the defined regions with the median (red line), average (black dot), 25th and 75th percentiles (blue box), and ±2.7 times the standard deviation (whiskers) indicated.

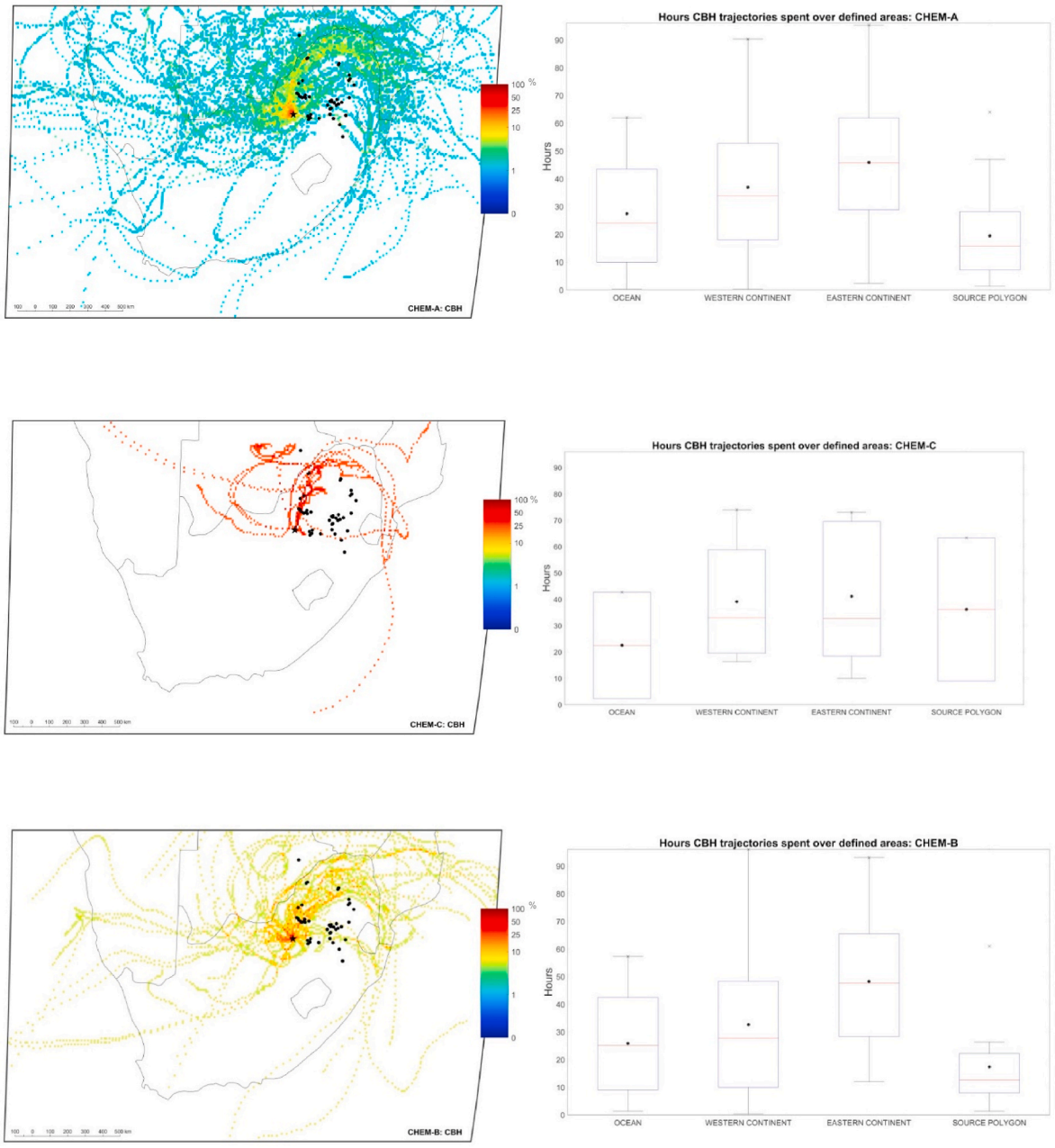

Fig. 3. 96-h overlay back trajectories for air masses arriving at CBH for each rain event in cluster CHEM-A, CHEM-B and CHEM-C at Welgegund. The colour scale bar presents the frequency (percentage) of air masses passing over a region. Boxplots presents the total time that air masses at the two arrival heights spent over the defined regions with the median (red line), average (black dot), 25th and 75th percentiles (blue box), and ±2.7 times the standard deviation (whiskers) indicated.

contributing to the observed differences in the VWM concentrations. In addition, increased rain intensity also corresponded to higher VWM concentrations. It has been indicated that scavenging ratios are usually higher for larger atmospheric particles (Galloway et al., 1993; González and Aristizábal, 2012). Kulshrestha et al. (2009), for example, reported that a shorter, more intensive rainfall event more effectively removed coarser particles from the atmosphere. González and Aristizábal (2012) indicated a positive correlation between scavenging ratios of SO_4^{2-} and NO_3^- and rain intensity. In a study conducted in China by Zhao et al. (2015), it was shown that larger particles (500–1000 nm) were effectively scavenged through thunderstorms, whereas smaller particles (10–50 nm) were more effectively scavenged through rain events with longer durations and lower raindrop velocities. Thunderstorms are commonly associated with larger raindrop size distribution and higher rainfall intensities, which could explain the more efficient scavenging (Zhao et al., 2015). Xu et al. (2017) also related higher below-cloud scavenging with increased rain intensity.

3.2. Clustering air mass history

Clustering according to the ionic composition of rainwater did not distinctly reveal the influences of sources on rain chemistry. Therefore, a different approach was followed where air mass history was clustered and possible differences in the chemical composition of rainwater were assessed. The average time that air masses arriving at Welgegund at 100 m a.g.l. and CBH spent over different defined source regions (Fig. 1) was clustered in this approach.

3.2.1. 100 m a.g.l. arrival height

In Fig. 4, clustering according to the time that air masses arriving at

100 m a.g.l. spent over the defined source regions prior to arrival at Welgegund are presented. The three clusters, i.e. 100m-A, 100m-B and 100m-C comprised 43, 34 and 23% of all rain events, respectively. Clusters 100m-B and 100m-C represented air masses spending significantly more time over the eastern source regions, with air masses in cluster 100m-B spending more time over the eastern source region including the large point sources, and 100m-C spending more time over the eastern source region excluding the large point sources. Air masses in these two clusters spent very little time over the oceans and the clean western background region. Cluster 100m-A represents air masses spending more time over oceans and the clean western background regions, and less time over the eastern source region in comparison to clusters 100m-B and 100m-C. Overlaid back trajectories of air mass movements in each of these clusters are presented in Figure A2.

The chemical composition of rain samples in each of the three clusters obtained for air mass history at a 100 m arrival height are presented in Table 2 together with the pH, EC and ancillary measurements associated with each cluster. Cluster 100m-A had the highest total VWM concentrations of ionic species. It is also of interest to note that cluster 100m-A and 100m-B had similar rain depths, which indicate that observed differences in VWM concentrations of ionic species in rainwater were indicative of the influence of different sources. Furthermore, cluster 100m-C had the lowest total VWM concentrations associated with the lowest rainfall depth. VWM concentrations of Na^+ and Cl^- generally associated with oceanic air masses were the highest in cluster 100m-A. Ca^{2+} and Mg^{2+} levels were also significantly higher in this cluster, which can indicate the influence of crustal sources from the clean western background region (Figure A2). VWM concentrations of Mg^{2+} and K^+ that are mainly associated with oceanic or crustal sources (Kok et al., 2021; Conradie et al., 2016; Sun et al., 2010) were also higher in cluster 100m-A. Relatively higher Ca^{2+} and Mg^{2+} concentrations in cluster 100m_B can possibly be attributed to fly ash emissions from industrial activities (Laakso et al., 2012). Cluster 100m-B had the highest H^+ levels, which is indicative of the influence of large point sources on rain chemistry, as well as decreased neutralisation of acidic species by Ca^{2+} for air masses associated with this cluster. However, relatively small differences in the average pH of rain events in the three clusters were evident. Furthermore, the VWM concentrations of anthropogenic acidic species, i.e. SO_4^{2-} and NO_3^- were similar in all three clusters, which signify the regional impacts of anthropogenic activities in the north-eastern interior on rain chemistry as indicated by Kok et al. (2021). SO_4^{2-} levels were, however, marginally higher in cluster 100m-B. NO_3^- levels were higher in clusters 100m-A and 100m-C, which also point to the regional impacts of household combustion for space heating and cooking. Cluster 100m-A also had the highest VWM concentrations of species typically associated with biomass burning, i.e. OAs, K^+ and Cl^-, while CO and eBC levels were also slightly higher in cluster 100m-A. 21% of the rain events in cluster 100m-A coincided with the biomass burning season (mid-May to mid-October) (Kok et al., 2021). NH_4^+ levels in all three clusters reflect the influence of local and regional agricultural activities on atmospheric processes in this part of South Africa.

No real significant differences were observed between the ancillary measurements in each of the back trajectory clusters. Mean SO_2 concentrations in cluster 100m-B were marginally higher than levels thereof associated with the other two clusters. Similar concentration of NO_x in all three air mass clusters also emphasize the influence of anthropogenic activities on air quality in this region. In contrast to the clustering according to ionic composition of rain, rain intensity had no significant correlation to observed differences in the three 100 m a.g.l. air mass arrival height clusters. The lowest average CBH 15 min prior to a rain event in cluster 100m-A also corresponded to higher total VWM concentrations than observed for cluster CHEM-C (Section 3.1). Analysis of variances of the ionic composition and ancillary measurements in these three clusters only revealed statistically significant variances and effect sizes concerning H^+ concentrations between cluster 100m-B and the other two clusters. Trajectory analyses at an arrival height of 100 m a.g.l. confirmed the influence of residence time of air masses over source regions on the variability in rainwater chemistry. Movement of air masses over the major point sources in 100m-B, similar to that of CHEM-B, are related to higher SO_4^{2-} concentrations and low pH, which are associated with anthropogenic activities.

3.2.2. Cloud base arrival height

Cluster solutions according to the time that air masses arriving at CBH spent over the defined source regions prior to a rain event at Welgegund are presented in Fig. 5. As mentioned, three clusters labelled CBH-A, CBH-B and CBH-C were determined which contained 34, 43 and 23% of all rain events. Cluster CBH-A contained air masses predominantly passing over the clean western background region and western oceans, with <8% of back trajectories passing over the eastern source regions and no back trajectories passing over the region wherein the large point sources are located. Air masses in cluster CBH-B spent significantly more time over the eastern source region, excluding the large point sources, with very few air masses passing over oceans. Cluster CBH-C represents air masses passing predominantly over the eastern continent (including and excluding large point sources), while air masses also spent time over eastern oceanic regions. In Figure A3 overlaid back trajectories of these air masses at CBH in the three different clusters are presented.

The chemical composition of rain samples in each of the three clusters obtained for air mass history at CBH are presented in Table 3 together with the pH, EC and ancillary measurements associated with each cluster. Based on the clustering according to air masses arriving at CBH, CBH-A, representing air masses spending most time over the clean western background region, had the highest total VWM concentrations of ionic species. However, the total VWM concentrations of ions in cluster CBH-B were marginally lower, which could be attributed to

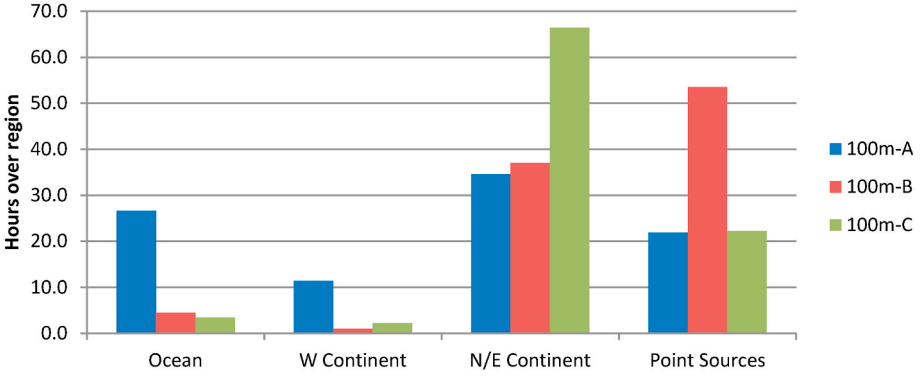

Fig. 4. Time air masses at a 100 m a.g.l. arrival height spent over defined source regions in each cluster.

Table 2
Air mass history clustering at 100m arrival height: VWM concentrations (μeq.L^{-1}) of ionic species in each cluster, as well as average pH, electrical conductivity (EC), rainfall depth and ancillary measurements. The standard deviations are indicated in brackets.

	100m-A		100m-B		100m-C	
# of samples	37		29		20	
H^+	20.68	[16.07]	36.49	[30.67]	28.77	[29.78]
Na^+	25.82	[35.98]	19.7	[55.23]	11.12	[10.47]
NH_4^+	28.14	[23.80]	23.76	[15.77]	29.02	[16.26]
K^+	9.8	[14.67]	5.77	[19.48]	4.73	[4.44]
Mg^{2+}	19.95	[65.15]	14.43	[59.53]	4.64	[3.77]
Ca^{2+}	38.63	[64.28]	22.96	[46.59]	17.03	[10.63]
NO_3^-	35.81	[59.45]	30	[32.50]	34.66	[17.09]
Cl^-	25.75	[32.63]	19	[56.38]	11.18	[8.59]
SO_4^{2-}	50.85	[37.23]	52.28	[32.51]	46.47	[29.14]
F^-	0.51	[0.64]	0.79	[0.93]	0.47	[0.30]
tOA*	16.8	[20.57]	6.26	[19.53]	7.4	[8.89]
Total VWM	272.75		231.45		195.49	
pH	4.87	[0.71]	4.81	[0.88]	4.76	[0.53]
EC (μS)	33.19	[26.94]	46.53	[55.52]	26.34	[24.28]
O_3 (ppb)	32.47	[11.93]	32.82	[10.65]	31.54	[9.45]
SO_2 (ppb)	0.8	[1.64]	1.25	[2.85]	0.44	[0.66]
NO (ppb)	0.06	[0.16]	0.04	[0.21]	0.1	[0.34]
NO_x (ppb)	2.72	[2.62]	2.76	[2.65]	2.85	[1.96]
CO (ppb)	135.99	[41.97]	124.25	[32.59]	116.66	[34.95]
PM_{10} (μg.m^{-3})	16.6	[10.06]	14.34	[9.79]	16.93	[16.33]
eBC (μg.m^{-3})	0.4	[0.38]	0.3	[0.52]	0.26	[0.37]
Total rain depth (avg) (mm)	570 (15.41)	[14.27]	631 (21.74)	[19.32]	240 (11.98)	[7.03]
Average (max) rain intensity (mm.h^{-1})	4.92 (15.10)	[4.00] [12.36]	4.92 (19.92)	[4.24] [20.21]	3.62 (13.66)	[11.46] [2.43]
CBH_2hr (m)	2332.3	[1081.42]	2075	[835.49]	2632.5	[791.08]
CBH_15min (m)	1835.14	[785.13]	1735.17	[899.97]	2358.95	[814.11]

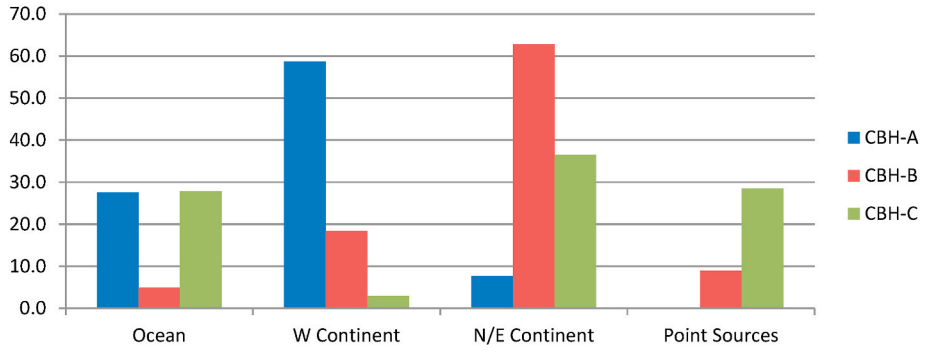

Fig. 5. Time air masses at CBH spent over defined source regions in each cluster.

higher rainfall depth recorded for rain events in this cluster compared to cluster CBH-A. Cluster CBH-C had the lowest total VWM concentrations associated with rainfall depth, similar to that of cluster CBH-A. VWM concentrations of Na^+, Cl^-, Mg^{2+}, Ca^{2+}, NO_3^- and SO_4^{2-} were the highest for rain events grouped in cluster CBH-A, with Ca^{2+} levels being significantly higher. Rain events in CBH-B had the highest H^+ and corresponding lowest pH, which are most likely due to significantly lower Ca^{2+} in comparison to levels thereof in rain grouped in cluster CBH-A. The extent of neutralisation of rain at Welgegund by Ca^{2+} is also signified by clustering of these air masses. Although the concentrations of species typically associated with oceanic air masses, i.e. Na^+ and Cl^-, were higher in cluster CBH-A, no noteworthy difference was observed compared to levels thereof in the other clusters. Higher concentrations of Cl^- and K^+ in cluster CBH-B that has the least frequent impacts by oceanic air masses, together with the highest total OA VWM concentrations in this cluster, are indicative of the influence of biomass burning on rain chemistry. Higher concentrations of anthropogenic acidic species, i.e. SO_4^{2-} and NO_3^- in cluster CBH-A and CBH-B in comparison to cluster CBH-C, which represents air masses at CBH spending more time over the point sources, points to the regional influence of anthropogenic activities in this region. Since higher concentrations of these anthropogenic species are associated with air masses at CBH passing over a relatively clean background region prior to a rain event, below-cloud scavenging can be considered more important in influencing the chemical composition of rain in this part of South Africa. Xu et al. (2017) showed that SO_4^{2-} deposited during the initial moments of a rain event corresponded to concentrations thereof in ambient aerosols. Furthermore, higher concentrations of Na^{2+} and Cl^- in cluster CBH-B, representing air masses spending <8% over oceans, also point to the more prominent influence of below-cloud air mass movement and -scavenging.

Comparison of ancillary measurements associated with rain events in

Table 3
Air mass history clustering at CBH arrival height: VWM concentrations (μeq.L^{-1}) of ionic species in each cluster, as well as average pH, electrical conductivity (EC), rainfall depth and ancillary measurements. The standard deviations are indicated in brackets.

	CBH-A		CBH-B		CBH-C	
# of samples	29		37		20	
H^+	19.7	[17.41]	36.67	[27.77]	24.93	[22.60]
Na^+	24.58	[38.44]	19.12	[50.10]	17.3	[35.94]
NH_4^+	26.97	[21.22]	31.73	[19.53]	16.09	[13.46]
K^+	7.65	[16.50]	8.15	[15.82]	4.81	[15.40]
Mg^{2+}	23.59	[71.68]	6.65	[10.52]	16.94	[74.72]
Ca^{2+}	39.79	[62.66]	21.88	[21.22]	23.42	[65.61]
NO_3^-	41.41	[40.71]	31.94	[18.98]	23.37	[36.45]
Cl^-	23.32	[37.43]	20.59	[52.70]	15.5	[29.11]
SO_4^{2-}	53.68	[37.22]	52.02	[24.13]	43.13	[38.70]
F^-	0.47	[0.49]	0.6	[0.57]	0.77	[1.09]
tOA*	9.84	[20.62]	15.58	[22.30]	3.57	[5.97]
Total VWM	271.01		244.94		189.83	
pH	5.04	[0.80]	4.65	[0.50]	4.91	[0.87]
EC (μS)	35.62	[36.37]	34.9	[39.54]	33.99	[40.31]
O_3 (ppb)	35.68	[8.99]	34.07	[10.14]	23.99	[11.61]
SO_2 (ppb)	0.55	[0.72]	0.79	[1.64]	1.67	[3.46]
NO (ppb)	0	[0.13]	0.06	[0.17]	0.24	[0.48]
NO_x (ppb)	2.05	[1.57]	2.97	[2.24]	3.86	[3.98]
CO (ppb)	117.07	[37.47]	129.39	[36.42]	140.12	[37.16]
PM_{10} (μg.m^{-3})	15.56	[11.76]	16.31	[11.34]	15.75	[12.06]
eBC (μg.m^{-3})	0.25	[0.28]	0.39	[0.37]	0.38	[0.66]
Total rainfall depth (avg) (mm)	424.00 (14.62)	[13.01]	611.50 (16.53)	[14.82]	442.50 (22.13)	[19.11]
Average (max) rain intensity (mm.h^{-1})	5.88 (18.30)	[4.91] [16.77]	4.43 (15.69)	[3.00] [10.05]	3.55 (18.40)	[2.73] [20.42]
CBH_2hr	2741.72	[861.62]	2296.22	[776.03]	1606.5	[1060.65]
CBH_15min	2189.29	[905.68]	1930	[739.44]	1415.26	[878.01]

these clusters obtained for air masses arriving at CBH, indicate that mean concentrations of species associated with anthropogenic activities, i.e. SO_2, NO_x and CO, were higher in cluster CBH-C. However, average PM_{10} and eBC concentrations were similar in all three clusters although the time air masses spent over point sources differed, which also signify the influence of below-cloud scavenging on rain chemistry measured at Welgegund. Furthermore, since air masses associated with the highest SO_2 and NO_x ambient concentrations corresponded to rainfall with relatively lower SO_4^{2-} and NO_3^- VWM concentrations, it is also indicative that in-cloud oxidation of SO_2 and NO_x has a smaller contribution to rain chemistry. It is generally considered that between 48% and 84% of all the SO_2 conversion to H_2SO_4 in the troposphere occurs within clouds (Halsall, 2003), which is not that evident in rainwater chemistry when events are clustered according to air mass history at CBH. Furthermore, NO_x are not highly water-soluble and are not easily absorbed into cloud water (Finlayson-Pitts and Pitts, 2000). Similarly to that observed for cluster analysis according to the chemical composition of rain, average rain intensities in the three clusters determined for air masses arriving at CBH corresponded to total VWM concentrations of ionic species in each cluster, with the average rain intensity being the highest in cluster CBH-A. Lower O_3 concentrations in cluster CBH-C, are also expected due to titration of atmospheric O_3 within proximity of NO_x sources (Laban et al., 2018). EC measurements of rain events in each cluster correspond to the total VWM concentrations. Analysis of variance of ancillary measurements in these three clusters only revealed significant statistical and substantive variances for O_3 and NO concentrations in cluster CBH-C compared to the other two clusters.

Similarly to the clustering of the chemical composition of rain events, although some differences in ionic composition could be observed in the three clusters determined for air masses arriving at 100 m a.g.l. and CBH, statistical analysis did not explicitly reveal distinct differences between the ionic compositions associated with air masses passing over different source regions. However, the important influence of below-cloud scavenging on rain chemistry in this region was evident as indicated by relating air masses arriving at 100 m a.g.l. to the chemical composition of rain.

3.3. Comparing synoptic patterns

This section aims to explore the relationship between rain events associated with different synoptic systems at the mesoscale. Analysing synoptic charts could give some indication of the type of convection on the rain event day, in contrast with the 96-h back trajectories determined in the previous sections which incorporated the progression of synoptic patterns and the influence thereof on surface flow. All rain events were characterized by a surface trough extending from the north. Surface troughs associated with tropical disturbances can be related to strong convective rainfall, which are often associated with high rain intensities and -depths (in many instances thunderstorms) over the plateau in the austral summer (Mogale and Dyson, 2017; Tyson and Preston-Whyte, 2017). Lynn et al. (2005) have reported that convective clouds scavenge 60% of the available CCN, with the most CCN scavenged within the first 30 min of cloud formation. Some rain events in this study corresponded to a coastal low pressure in addition to the surface trough, while there were also rain events that were characterised by westerly waves that are associated with cold fronts passing over this region from the south-west to the south-east. Coastal lows and westerly waves are temperate perturbations to the stable conditions that prevail over continental South Africa. Westerly waves typically advect polar maritime air from behind the cold front, and cloud bands commonly form through convection. Rainfall associated with these types of temperate westerly waves has relatively low rainfall intensities (Tyson and Preston-Whyte, 2017). Rain events related to surface troughs, coastal low pressures and westerly waves disturbances represented 49,

33 and 17%, respectively of the rainfall events collected at Welgegund.

In Table 4, the VWM concentrations of ionic species in rain events associated with each of the three synoptic systems are listed. In Figure A4 CBH, rain depth and -intensity, pH and EC of collected rain samples, as well as other ancillary measurements related to the three synoptic systems are presented. In general, rain events corresponding with coastal low pressures had the highest VWM concentrations of ionic species, while the lowest VWM levels were determined for rain events associated with westerly waves. In addition, higher average concentrations of CO, O_3, eBC and PM_{10}, highest average pressure, as well as the largest difference 2-h and 15-min averages of CBH corresponded with rain events related to coastal low pressures (Figure A4). These rain events also had the smallest rainfall depth. Events related to westerly wave disturbances and cold fronts had the lowest rain intensity, which could, as indicated above, contribute to lower VWM concentrations of ionic species. Small differences between the 2-h and 15-min CBH averages, and the narrow pressure range reflect large-scale cloud bands associated with these type of rain events corresponding to low rainfall intensity with longer duration (Figure A4). These rain events did, however, had the highest H^+ levels, which can be ascribed to significantly lower Ca^{2+} and Mg^{2+} concentrations. In addition, relatively higher VWM concentrations of NO_3^-, SO_4^{2-} and NH_4^+ in rain events associated with westerly waves can be attributed to higher relative humidity contributing to the scavenging of hygroscopic aerosols e.g. $(NH_4)_2SO_4$ (Figure A4). Westerly wave rain events also corresponded to the lowest average concentrations of SO_2, NO_x, CO and eBC, but the highest O_3 concentrations (Figure A4). The highest SO_4^{2-} VWM concentrations were determined in rain events related to surface troughs. However, neutralisation with species such as Ca^{2+} and NH_4^+ is reflected by low H^+ levels (and the higher pH). These rain events also coincided with the highest EC, SO_2 and NO_x concentrations, while these events also had high rainfall intensities (Figure A4).

3.4. Inter-comparison of rain event clustering

The three-cluster solutions determined with the different approaches in this study were inter-related in order to establish whether rain events grouped in one cluster according to a specific approach also occurs in a cluster determined with another approach. Clusters determined by grouping of the air masses at 100 m a.g.l. arrival heights suggested a statistical overlap with clusters obtained by grouping according to the ionic composition of rain, i.e. $p = 0.059$. Therefore, rain events grouped together according to ionic composition of rain events could also be clustered together when events are clustered according to air mass history at an arrival height of 100 m a.g.l. However, the clusters determined for air masses at CBH did not statistically correspond to any clusters determined for air masses arriving at 100 m a.g.l. or with clusters determined for the chemical composition of rain events, i.e. $p = 0.239$ and 0.874, respectively. Therefore, inter-comparison between different clustering approaches also reflects the significance of below-cloud scavenging on chemical composition of rain samples collected at Welgegund.

Table 4
VWM concentrations ($\mu eq.L^{-1}$) of ionic species associated with rain events corresponding to three dominant synoptic patterns. Standard deviations are indicated in brackets.

	Surface Troughs		Coastal Lows		Westerly Waves	
# of samples	47		32		17	
H^+	28.00	[26.00]	25.97	[15.25]	36.10	[36.51]
Na^+	20.85	[51.85]	21.66	[24.77]	14.99	[20.05]
NH_4^+	23.87	[18.39]	31.66	[21.98]	22.75	[11.85]
K^+	6.93	[18.63]	8.18	[11.69]	4.87	[4.47]
Mg^{2+}	12.86	[53.18]	22.19	[68.77]	3.44	[5.12]
Ca^{2+}	27.05	[54.66]	32.38	[50.04]	15.30	[16.29]
NO_3^-	29.96	[31.62]	40.03	[35.27]	26.66	[20.43]
Cl^-	20.29	[31.62]	21.41	[35.27]	15.43	[20.43]
SO_4^{2-}	51.50	[35.05]	47.75	[30.50]	43.46	[31.52]
F^-	0.69	[0.87]	0.47	[0.57]	0.40	[0.34]
tOA*	9.00	[21.90]	15.11	[14.14]	7.42	[8.98]
Total VWM	231.02		266.80		190.83	

The events in the three synoptic groups were also compared to the clusters determined according to the ionic composition. The amount of overlap between the compositional and 100 m a.g.l. air mass history clusters showed noteworthy similarities to the amount of overlap between the compositional and synoptic groups. This could indicate the influence of convection type on rainwater chemistry. The overlap between the chemical clusters and synoptic patterns could signify the relationship of certain ancillary measurements, which showed statistically significant differences between the groups within the HCA clusters, with the rainfall type or type of uplift associated with the precipitating cloud. These included maximum rainfall intensity, pressure, average CBH, RH, wind speed and temperature. However, the mesoscale factors influencing rain chemistry are complex and a definitive relationship between the type of convection and rainwater chemistry could not be established in the scope of this study. Modelling studies or field measurement studies of convection processes such as those by Tost et al., 2007); Fuentes et al. (2016) could be more appropriate to determine these relationships. The nuances between the synoptic pattern progression and surface flow determined through trajectories appear to be a better method to link surface air flow and rainwater chemistry.

In view of the results of the clustering analysis of rain chemistry and air mass history at Welgegund, the influences of different source regions, below-cloud scavenging, rain intensity and pollution build-up were further explored in the subsequent section by conducting case studies of specific rain events. Here the advantages associated with the availability of CBH measurements in conjunction with rain sampling is further investigated.

3.5. Case studies

In these case studies, rain events are assessed by presenting the ionic composition together with the event air mass histories arriving at Welgegund at 100 m a.g.l. and CBH. In each of the back trajectory maps presented in this subsection, 96-h back trajectories calculated at the median CBH prior to the rain event are plotted in gold, while blue lines represent the 96-h back trajectories with a 100 m a.g.l. arrival height. The Welgegund atmospheric research station is represented as a black star, the large pollution point sources as black dots, the Johannesburg-Pretoria conurbation as an area shaded in grey, and the burn scar areas four days prior to the rain events shaded in red.

3.5.1. Anthropogenic sources

The influence of the densely populated eastern source region, where the major pollution point sources in the interior of South Africa are located, on rain chemistry determined at Welgegund is illustrated in two examples presented in this case study. In Fig. 6, back trajectories at CBH and 100 m a.g.l. calculated for rain events on 7 and 9 January 2015 are presented, while Table 5 lists the concentrations of ionic species associated with these rain events. It is evident from Fig. 6 that below-cloud air masses passed over the eastern source region prior to both rain events. The air masses associated with the CBH only passed over this source region on 7 January 2015, while air masses at CBH bypassed most of the eastern source region on 9 January 2015. Both rain events illustrate the influence of anthropogenic sources on the chemical composition, especially as indicated by the elevated levels of SO_4^{2-} and NO_3^-. Although the statistical analyses discussed previously did not point to a significant contribution of CBH on rain chemistry, this case study shows that air mass history associated with the precipitating cloud could contribute to the chemical composition as indicated by the higher SO_4^{2-} and NO_3^- concentrations in the event of 7 January 2015. These elevated concentrations are possibly related to both in-cloud scavenging processes and to the below-cloud pollutant scavenging that is explored in a

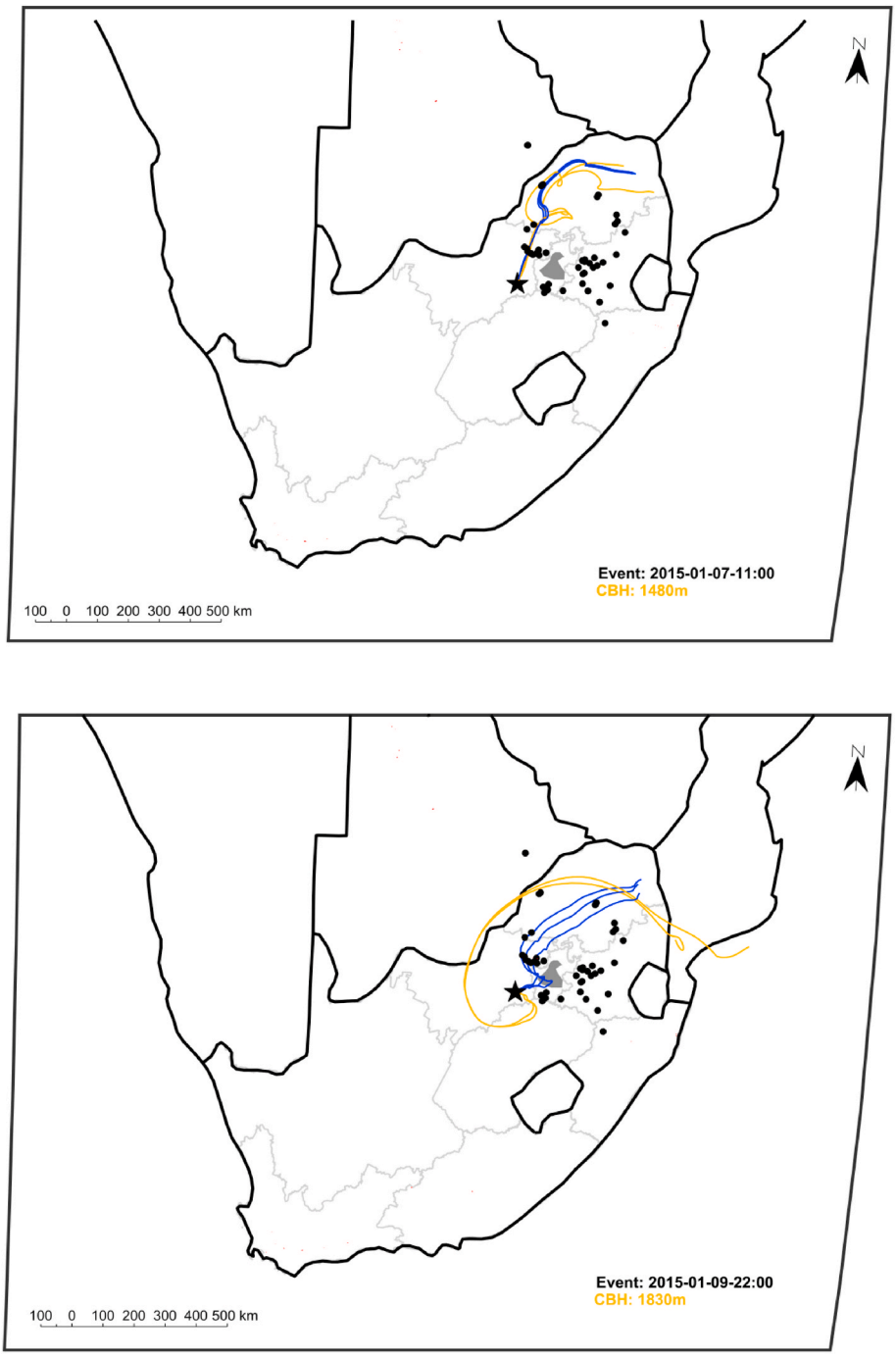

Fig. 6. 96-h back trajectories at CBH and 100 m a.g.l. indicating air mass movement over anthropogenic sources for rain events occurring on 7 January 2015 (top) and on 9 January 2015 (bottom).

following case study.

3.5.2. *Below-cloud scavenging*

The influence of below cloud scavenging is assessed through two case studies where the VWM concentrations of ionic species in rain samples collected during two sequential rain events are compared. In Tables 6 and 7 the rain chemistry for subsequent rain events in February 2017 and September 2015 are presented (air mass histories at CBH and 100 m a.g.l. of these rain events are presented in Figure A5 and A6). Air masses at CBH and 100 m a.g.l. passed over the eastern anthropogenic source region prior to the rain event on 20 February 2017. This rain event was followed up a few hours later on the next day with a rain event with similar air mass history at both arrival heights, as well as rain depth and -intensity. It is evident that the VWM concentrations of ionic species were lower in the rain event on 21 February 2017. The influence of below-cloud scavenging is also illustrated by two successive rain events on 4 and 5 September 2015, which also corresponded to similar air mass histories over the eastern source region. Here more significant differences in the VWM concentrations of ionic species were determined with levels of ionic species being substantially lower in rain on 5 September 2015, especially for VWM concentrations of SO_4^{2-}, NO_3^- and NH_4^+. This case study of successive rain events also presents examples of rain events that were grouped into different clusters according to chemical composition, while clustering according to air mass history grouped

Table 5
Rainwater ionic concentrations (μeq.L^{-1}), rain depth and -intensity associated with rain events on 7 and 9 January 2015.

	7 January 2015	9 January 2015
Rain depth (mm)	70.0	40.0
Max (avg) Intensity (mm.h^{-1})	92 (12.8)	51.2 (10.4)
pH	4.20	4.10
SO_4^{2-}	5285	3024
NO_3^-	2453	1444
NH_4^+	2442	1386
Ca^{2+}	1221	514
Mg^{2+}	442	68
Na^+	1670	95
Cl^-	1439	112
K^+	510	32
tOA*	17	14

Table 6
Rainwater ionic concentrations (μeq.L^{-1}), rain depth and -intensity for the rain events on 20 and 21 February 2017.

	20 February 2017	21 February 2017
Rain depth (mm)	60	38
Max (avg) Intensity (mm.h^{-1})	29.6 (5.6)	29.6 (3.8)
pH	4.99	5.07
SO_4^{2-}	1319	932
NO_3^-	350	270
NH_4^+	229	225
Ca^{2+}	285	289
Mg^{2+}	50	20
Na^+	136	118
Cl^-	141	128
K^+	56	14
tOA*	3	43

these events together. This also signifies the complexity associated with factors influencing rain chemistry and substantiates the suitability of the different statistical clustering approaches followed in this study.

3.5.3. Pollution build-up

During winter, an increase in the concentrations of chemical species in the atmosphere occur in the South African interior due more pronounced low-level inversion layers trapping pollutants near the surface in conjunction with anti-cyclonic recirculation of air masses through a persistent high-pressure system over this region (Laakso et al., 2012; Tyson and Preston-Whyte, 2017). In addition, increased household combustion for space heating and open biomass burning also contribute to additional emissions of atmospheric pollutants (Laban et al., 2018). Winter rainfall, although rare over the Highveld, can therefore have greater scavenging efficiencies (Tyson and Preston-Whyte, 2017). Two winter rainfall events that occurred on 13 June and 24 July 2016 are considered in this case study with the VWM concentrations of ionic species determined for these rain events presented in Table 8. Air mass history associated with these two rain events are shown in Figure A7. It is evident that rainwater collected in July had a much higher ionic load than the rain event in June. This increased scavenging of chemical species in the atmosphere by rainwater can be attributed to pollution build-up during winter since no rain events occurred between these two events. In addition, the air mass histories at the two arrival heights on 25 July 2016 spent a small amount of time over the eastern anthropogenic source region, signifying increased scavenging of atmospheric pollutants associated with pollutant build-up. The rain event on 4 September 2015 presented in the below-cloud scavenging case study above is also indicative of pollution build-up since it was the first event after winter and corresponded to higher concentrations of ionic species.

3.5.4. Rain intensity

The statistical analysis in the previous section indicated statistically

Table 7
Rainwater ionic concentrations (μeq.L^{-1}), rain depth and -intensity for the event on 4 September 2015 and a follow-up event on 5 September 2015.

	4 September 2015	5 September 2015
Rain depth (mm)	30	5
Max (avg) Intensity (mm.h^{-1})	4.8 (2.1)	1.6 (0.9)
pH	4.43	4.50
SO_4^{2-}	1273	211
NO_3^-	502	147
NH_4^+	559	97
Ca^{2+}	419	119
Mg^{2+}	138	46
Na^+	117	173
Cl^-	166	173
K^+	51	89
tOA*	456	197

Table 8
Rainwater ionic concentrations (μeq.L^{-1}), rain depth and -intensity associated with two rain events in winter in 2016.

	13 June 2016	24 July 2016
Rain depth (mm)	10	55
Max (avg) Intensity (mm.h^{-1})	8.8 (3.0)	23.2 (4.8)
pH	5.09	4.90
SO_4^{2-}	338	2931
NO_3^-	152	1672
NH_4^+	121	2168
Ca^{2+}	366	3112
Mg^{2+}	111	1137
Na^+	169	1518
Cl^-	171	1667
K^+	42	670
tOA*	184	2470

Table 9
Rainwater ionic concentrations (μeq.L^{-1}), rain depth and -intensity associated with the rain events with the highest maximum rain intensity (7 January 2015), the highest average rain intensity (28 February 2016), and the lowest average rain intensities (5 September 2015 and 18 December 2014).

	7 January 2015	28 February 2016	18 December 2014	5 September 2015
Rain depth (mm)	70	30	5	5
Max (avg) Intensity (mm. h^{-1})	92 (12.8)	66.4 (20.5)	1.6 (0.9)	1.6 (0.9)
pH	4.20	4.37	4.08	4.50
SO_4^{2-}	5285	2449	767	211
NO_3^-	2453	1173	503	147
NH_4^+	2442	1570	409	97
Ca^{2+}	1221	770	325	119
Mg^{2+}	442	187	112	46
Na^+	1670	481	490	173
Cl^-	1439	536	389	173
K^+	510	154	304	89
tOA*	17	221	14	93

significant differences for rain intensity in each of the clusters with higher VWM concentrations of ionic species associated with increased rain intensity. Therefore, in this case study, the rain events that had the highest average and maximum rain intensities are compared to two rain events with the lowest average rain intensities. In Table 9, the VWM concentrations of ionic species in the rain events that recorded the highest maximum rain intensity (7 January 2015), the highest average rain intensity (28 February 2016), and the lowest average rain intensities (5 September 2015 and 18 December 2014) during the sampling campaign are presented, while air mass histories at the two arrival heights for each of these rain events are presented in Figure A8. It is

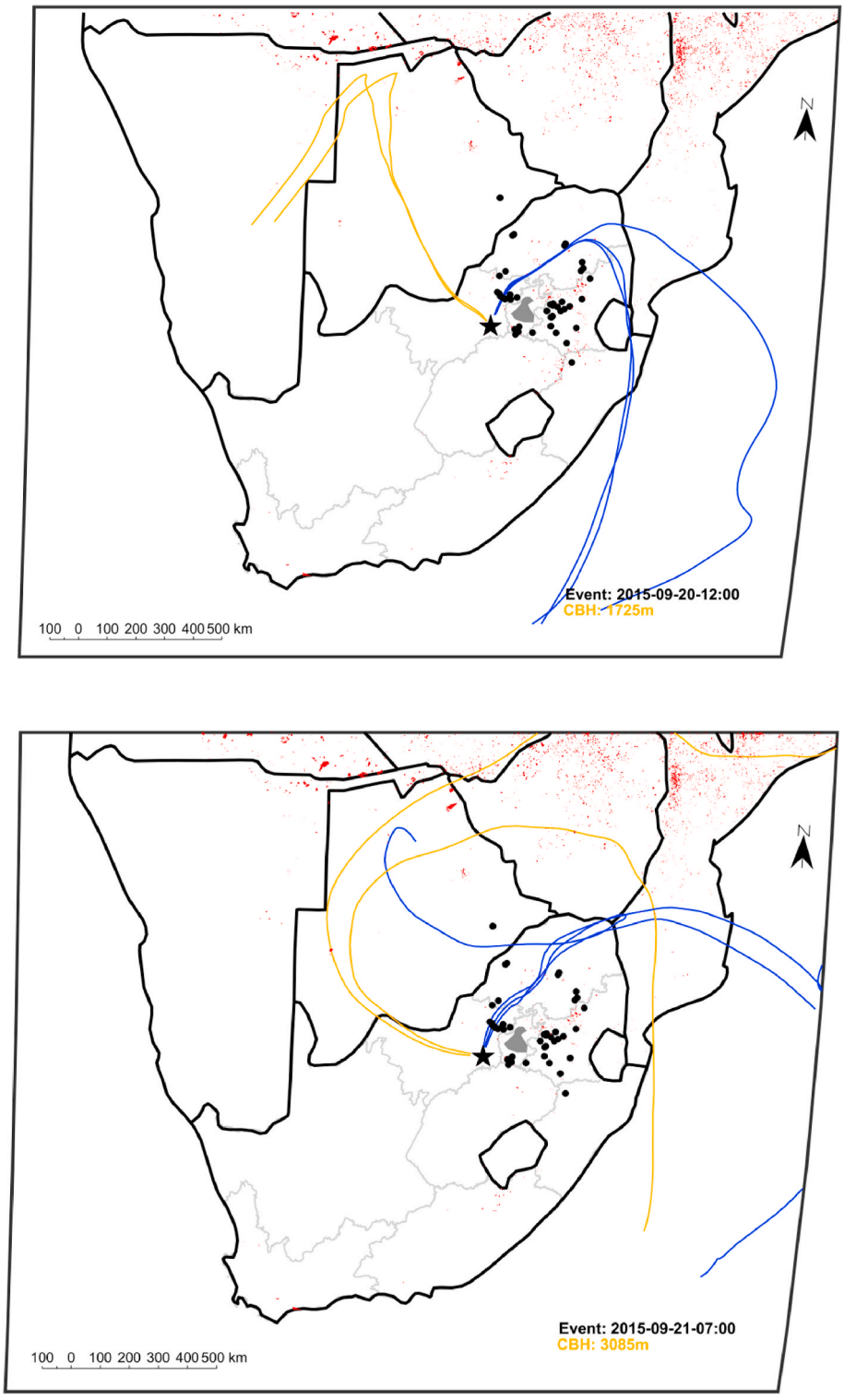

Fig. 7. Back trajectories at CBH and 100 m a.g.l. for rain events corresponding to open biomass burning.

Table 10
Rainwater ionic concentrations (μeq.L^{-1}), rain depth and intensity associated with two rain events during the peak open biomass burning season.

	20 September 2015	21 September 2015
Rain depth (mm)	11	13
Max (avg) Intensity (mm.h^{-1})	5.2 (2.0)	10.4 (4.6)
pH	4.49	4.51
SO_4^{2-}	513	583
NO_3^-	905	1049
NH_4^+	1108	1280
Ca^{2+}	424	452.5
Mg^{2+}	180	196
Na^+	630	680
Cl^-	913	1018
K^+	457	501
tOA*	548	594

evident that the rain events associated with higher rain intensities had significantly higher loadings of ionic species compared to the events related to lower rain intensities. The rain event with the highest maximum rain intensity recorded also had the highest measured rainfall depth of all rain events collected during this study. Furthermore, it is also apparent that air masses passed over the anthropogenic eastern source region prior to each of these rain events. Therefore, observed differences in chemical composition of rain cannot be attributed to different air mass histories. Strong convective rainfall over the Highveld often associated with high rain intensity, large rain depths, hail and thunderstorms has been related to increased scavenging (Wallace and Hobbs, 2006; Hart et al., 2013; Zhao et al., 2015; Mogale and Dyson, 2017).

3.5.5. *Open biomass burning*

Kok et al. (2021) indicated that the influence of open biomass burning on the chemical composition of rainwater was less pronounced due to the open biomass burning season not corresponding with the wet season on this part of South Africa. The open biomass burning season is typically from June to mid-October (Harrison, 1986). However, a case study is presented in order to show the possible influence of open biomass burning on rain chemistry. Open biomass burning is generally associated with emissions of OAs, while it can also be related to Cl^- and K^+ (Galy-Lacaux et al., 2009). In Fig. 7, the air mass histories associated with two rain events that occurred during the peak burning season on 20 and 21 September 2015 are presented, which indicate air masses passing over open biomass burning prior to these rain events. It is evident from the ionic concentrations determined for these two rain events, presented in Table 10, that air masses passing over open biomass burning contributed to increased levels of OAs, Cl^- and K^+ in rainwater. Elevated Cl^- levels from biomass burning are also supported by the Cl^- concentrations being higher than Na^+ levels, since concentrations of Na^+ and Cl^- are mostly similar in rain collected in this part of South Africa (Conradie et al., 2016; Kok et al., 2021). It is also evident form the air mass histories associated with these two rain events that the long-range transport of air masses passing over distant fires that do not occur during the open biomass burning season in South Africa can have an impact on precipitation chemistry in this region.

4. Summary and conclusion

The aim of this study was to conduct an advanced assessment on factors influencing chemical composition of rain in the South African interior by developing a novel method to relate rain events at Welgegund to air mass history at arrival heights below clouds and at CBH. HCA were performed following two different approaches, i.e. clustering based on the chemical composition of rain that was related to air mass histories at the two arrival heights, as well as grouping based on air masses arriving at 100 m a.g.l. and CBH that was then associated with chemical composition. Cluster solutions were also related to ancillary measurements conducted at Welgegund. In each of the approaches in this study, the optimum solutions yielded three clusters.

Clustering analysis was useful in establishing some correlations between rain chemistry and the source regions that air masses pass over prior to a rain event. Clustering conducted according to the ionic composition of rain events grouped rain events together in relation to their total VWM concentrations, i.e. from high to low VWM concentrations. Correlation of air mass histories to the three clusters indicated to an extent that higher VWM concentrations were associated with air masses at 100 m a.g.l. passing over anthropogenic source regions. Air mass history clustering grouped air masses passing predominantly over predefined source regions. The rain chemistry of clusters determined for air masses at 100 m a.g.l. arrival heights could mainly be related to the influence of large point sources, the clean western background sector and oceans. Clustering according to chemical composition and air masses with an arrival height of 100 m a.g.l. also reflected the regional impact of anthropogenic activities in the north-eastern part of South Africa. Although air masses arriving at CBH did partially contribute to rain chemistry, no significant correlations between air mass histories at CBH and ionic composition were evident. Therefore, it could be concluded from the statistical analysis that below-cloud atmospheric chemical composition was more significant in contributing to the chemical composition of rain in this part of South Africa.

Considering the surface synoptic charts and satellite imagery of the rain event days, rain events were categorised according to three main synoptic patterns. The highest total VWM was measured for events corresponding with coastal low pressures, while the lowest VWM was measured for rain events related to westerly wave disturbances. Events related to strong convective uplift, high rain intensity and -depth, and wind speed had the highest VWM concentrations. Since surface flow patterns vary greatly, even in the specific groups identified, it is concluded that surface flow trajectories are a more reliable method to relate air mass history to rainwater chemistry.

A few case studies are presented, in order to further illustrate factors influencing the chemical composition of rain in this part of South Africa. The influence of the anthropogenic source region on rain chemistry at Welgegund, as revealed through statistical analysis could be confirmed, while the effect of below-cloud scavenging on rain chemistry at Welgegund was highlighted through investigation of the chemical composition of successive rain events associated with similar air mass histories. A case study also revealed the impact of pollution build-up during winter, with rainfall associated this period corresponding to higher loading of ionic species. In addition, the correlation between higher ionic concentrations and increased rain intensity, as suggested by statistical analyses, was also supported. Finally, the impact of open biomass burning was also indicated, while it was also suggested that long-range transport of species associated with open biomass burning could influence rain chemistry in the South African interior.

Although statistical analyses could be successfully employed in this study, it also highlighted the complexity associated with correlating rain chemistry to sources of chemical species, as well as the limitations associated with statistical analyses of the entire datasets. It is recommended that future studies also consider other advanced statistical methods. Other input parameters could also be considered, e.g. upper atmospheric conditions. Some uncertainties can also be associated with the exact CBH during the onset of a rain event due to assumptions made in this study. In addition, there is also uncertainty associated with back trajectory analysis, which was mitigated through compiling three back trajectories for each rain event. However, it is recommended that future studies utilise newly developed and more advanced dispersion models, e.g. FLEXPART, to calculate air mass histories. Furthermore, microscale and mesoscale factors associated with the cloud environments could not be assessed in this study.

Authors' contributions

LK, were the main investigators in this study and wrote the manuscript. conducted this study as part of her PhD degree, as well as performed most of the experimental work and data processing. JPB, were the main investigators in this study and wrote the manuscript. The project was led by, PGvZ, were the main investigators in this study and wrote the manuscript. The project was led by, RPB, were the main investigators in this study and wrote the manuscript. The project was led by, MJ, which were also study leaders of the, assisted with sample collection and site maintenance, VV, which were also study leaders of the, assisted with sample collection and site maintenance, also made conceptual contributions. KJ, which were also study leaders of the, assisted with sample collection and site maintenance, SME, provided guidance with the statistical analysis. MK, provided financial support for the measurements, also made conceptual contributions. LL, also made conceptual contributions.

Declaration of competing interest

The authors declare that they have no known competing financial interests or personal relationships that could have appeared to influence the work reported in this paper.

Data availability

Data will be made available on request.

Acknowledgments

The authors acknowledge the following projects: ACCC Flagship funded by the Academy of Finland grant number 337549 (UH) and 337552 (FMI), "Gigacity" project funded by Wihuri foundation, European Research Council (ERC) project ATM-GTP Contract No. 742206. The authors also wish to thank the International Network to study Deposition and Atmospheric composition in Africa (INDAAF) network and the Atmospheric Research in Southern Africa and Indian Ocean (ARSAIO) programme for support. Jan-Stefan Swartz (Chemical Resource Beneficiation, North-West University, Potchefstroom, South Africa) for his assistance with ion chromatography analysis also acknowledged. This publication forms part of the output of the Biogeochemistry Research Infrastructure Platform (BIOGRIP) of the Department of Science and Innovation of South Africa, which supports the Welgegund station.

Appendix

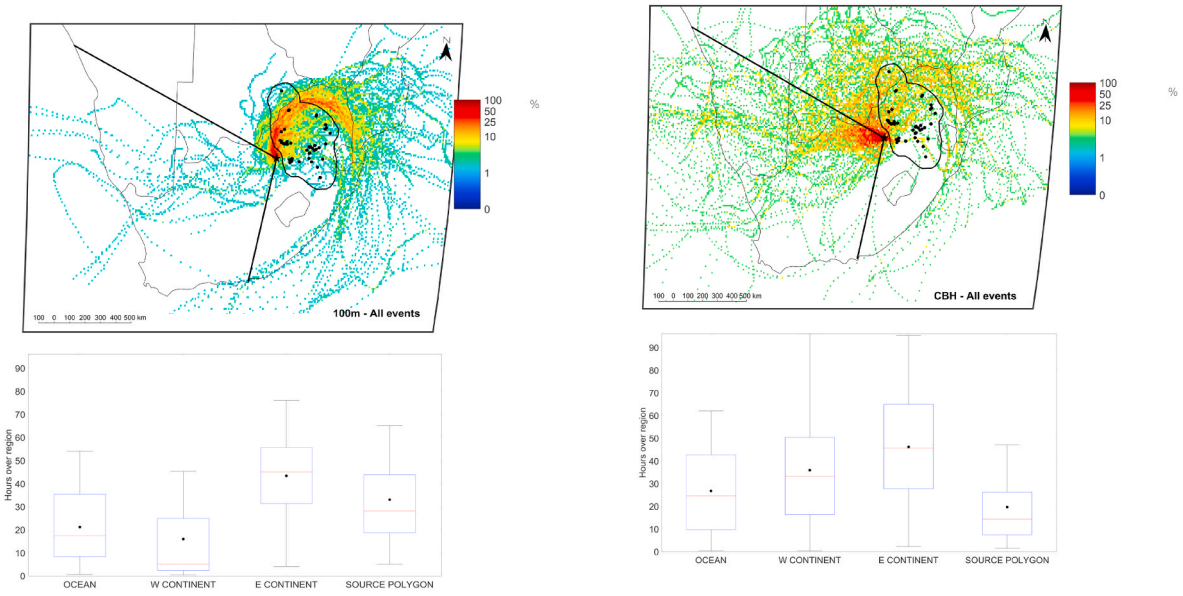

Fig. A1. 96-h overlay back trajectories for air masses arriving at 100m a.g.l. (left) and CBH (right) for each rain event at Welgegund. The colour scale bar presents the frequency (percentage) of air masses passing over a region. Boxplots presents the total time that air masses at the two arrival heights spent over the defined regions with the median (red line), average (black dot), 25th and 75th percentiles (blue box), and ±2.7 times the standard deviation (whiskers) indicated.

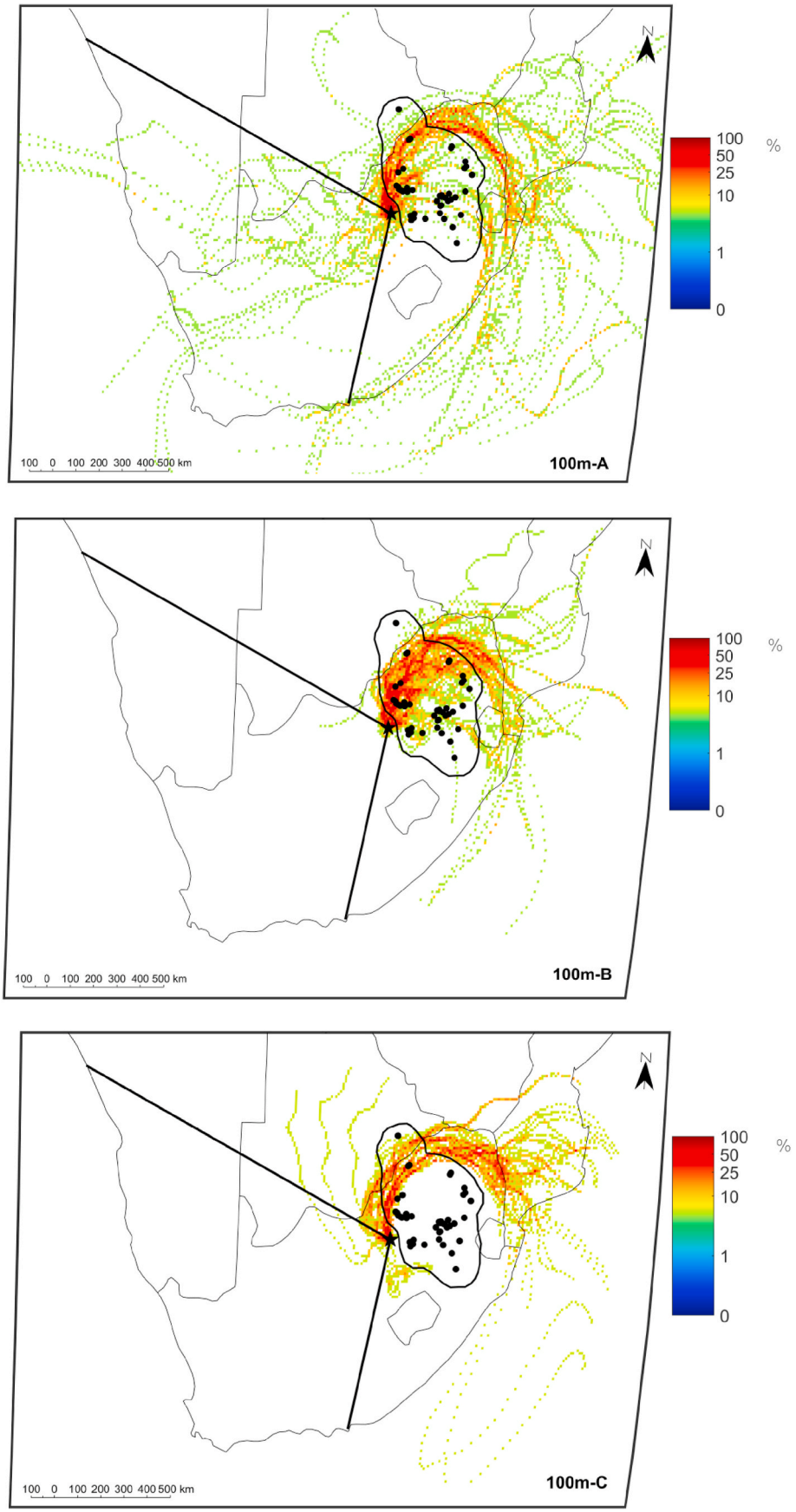

Fig. A2. 96-h overlay back trajectories for air masses clustered according to the time the air masses at 100 m a.g.l. arrival height spent over defined source regions. The colour scale bar presents the frequency (percentage) of air masses passing over a region.

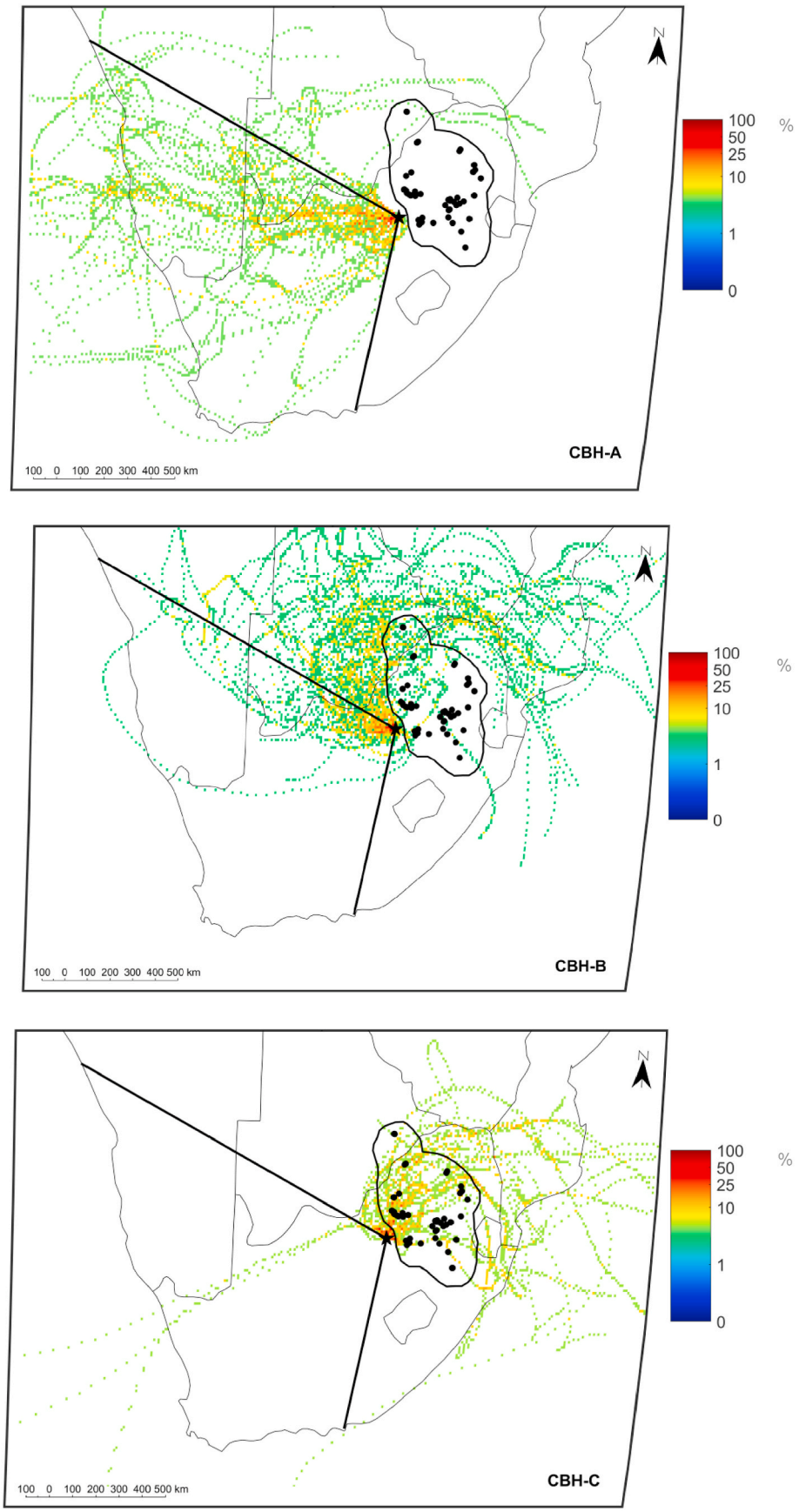

Fig. A3. 96-h overlay back trajectories for air masses clustered according to the time air masses at CBH spent over defined source regions. The colour scale bar presents the frequency (percentage) of air masses passing over a region.

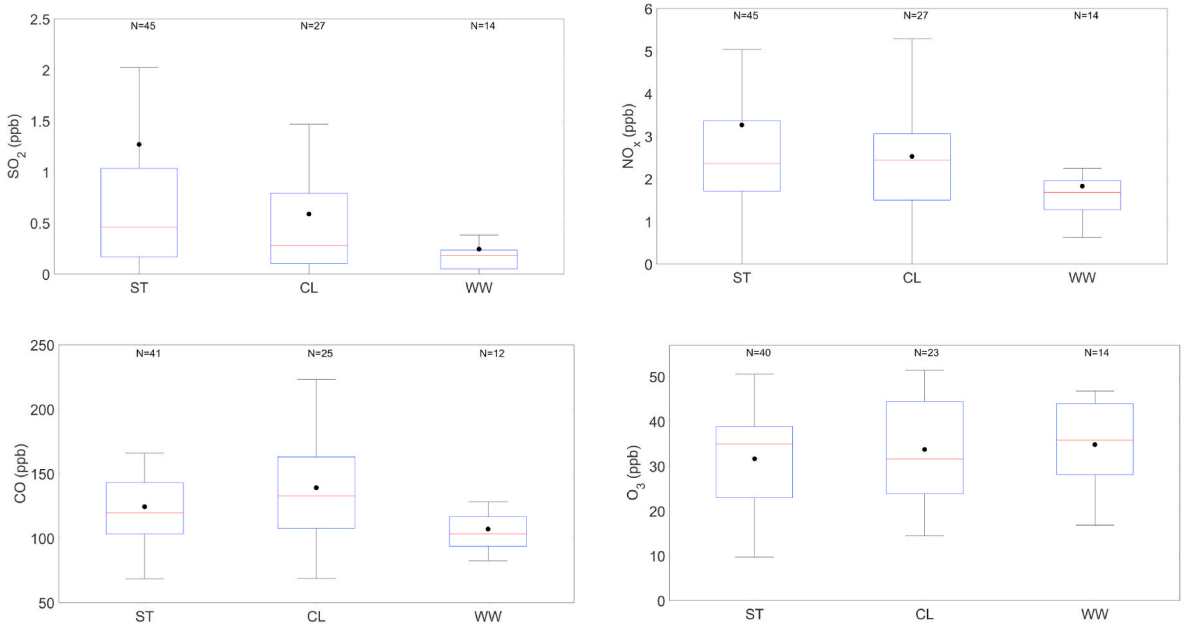

Fig. A4 (a). Average concentrations of gaseous species prior to rain events associated with three synoptic systems (ST: Surface Trough; CL: Coastal Low Pressure; WW: Westerly Waves).

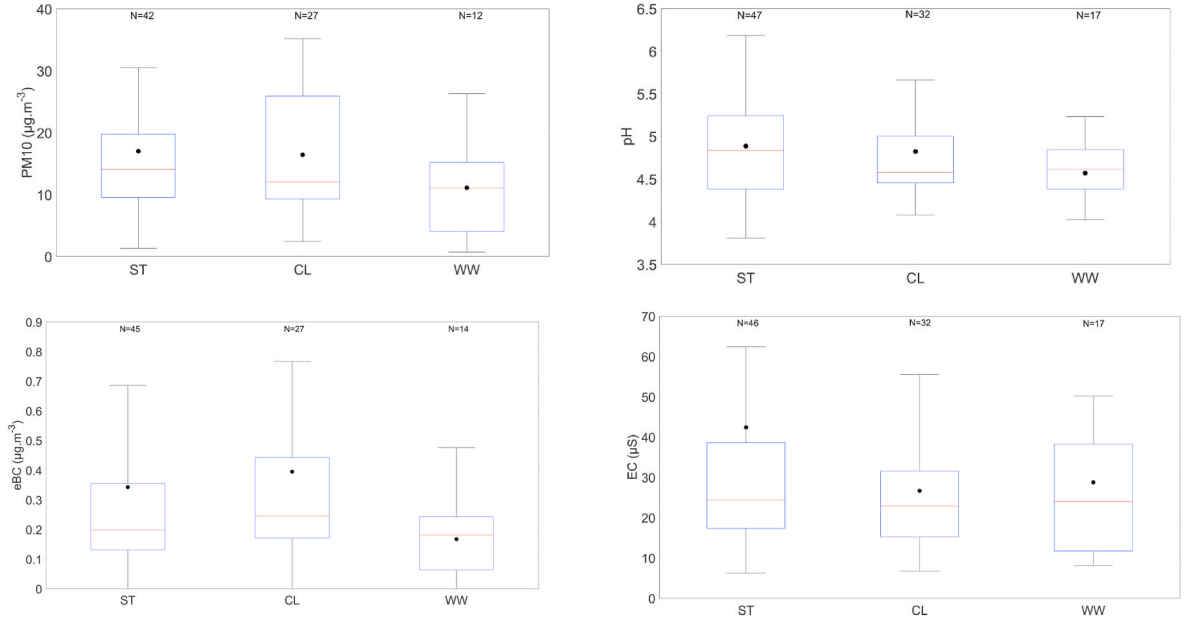

Fig. A4 (b). Average concentrations of PM_{10} and eBC prior to rain events, as well as the pH and EC of rain events associated with three synoptic systems (ST: Surface Trough; CL: Coastal Low Pressure; WW: Westerly Waves).

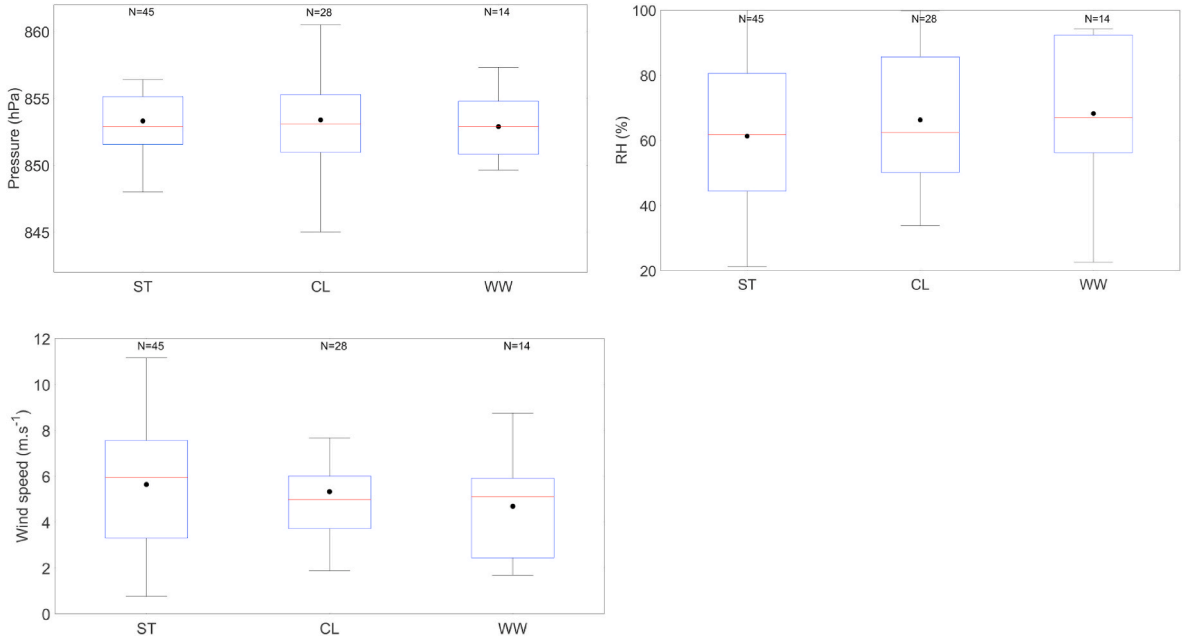

Fig. A4 (c). Average pressure, RH and wind speed prior to rain events associated with three synoptic systems (ST: Surface Trough; CL: Coastal Low Pressure; WW: Westerly Waves).

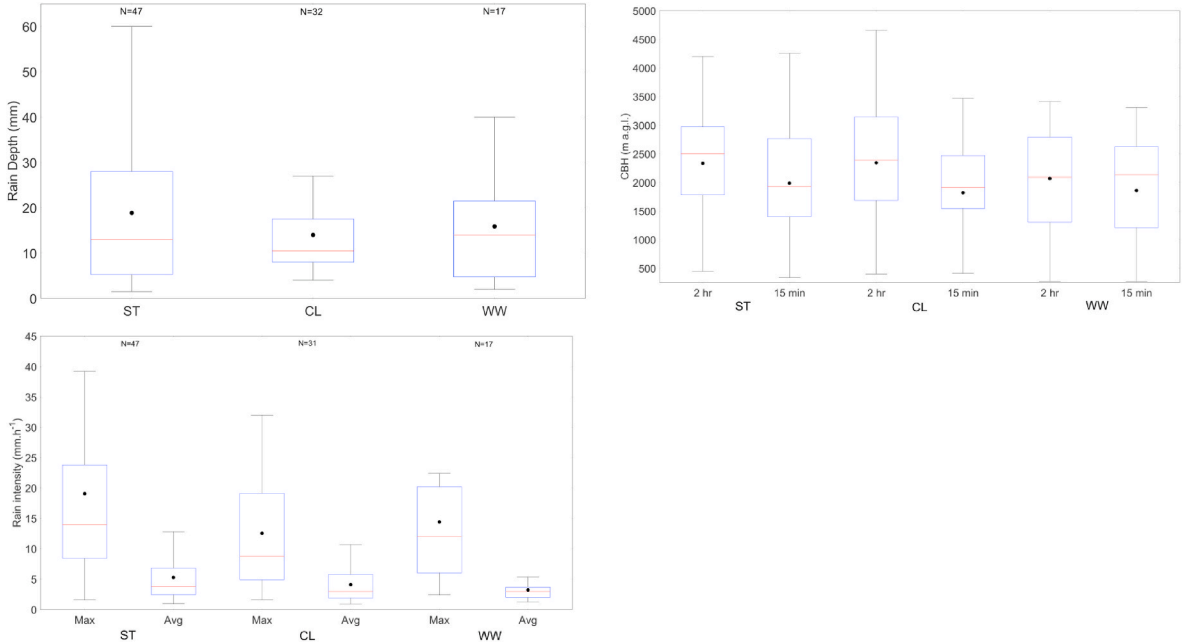

Fig. A4 (d). Rain depth and -intensity, as well as averaged 2-h and 15-min CBH measured for rain events associated with three synoptic systems (ST: Surface Trough; CL: Coastal Low Pressure; WW: Westerly Waves).

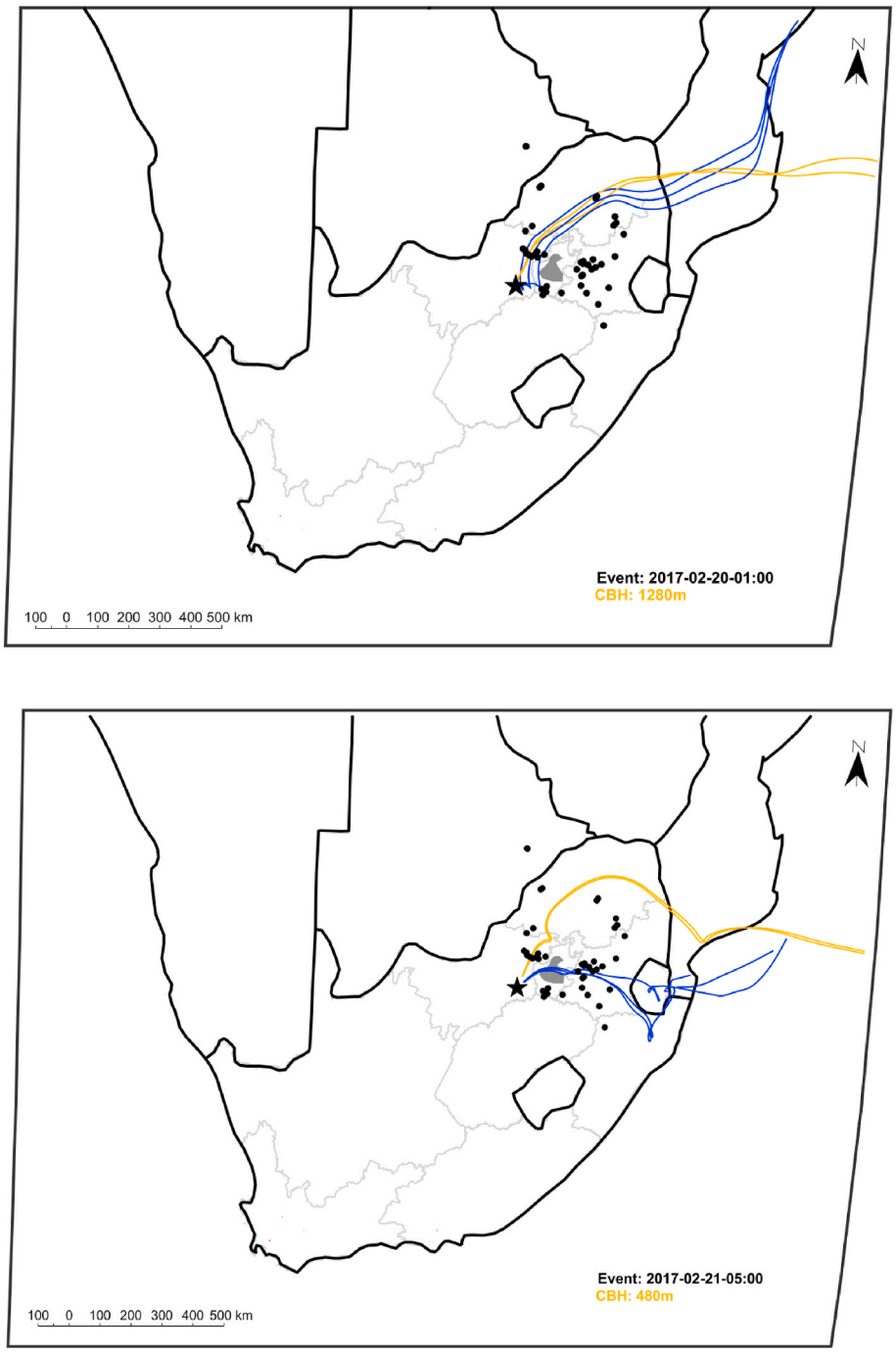

Fig. A5. Back trajectories at CBH and 100 m a.g.l. for rain events on 20 February 2017 (top) and 21 February 2017 (bottom), indicating below-cloud scavenging of pollutants.

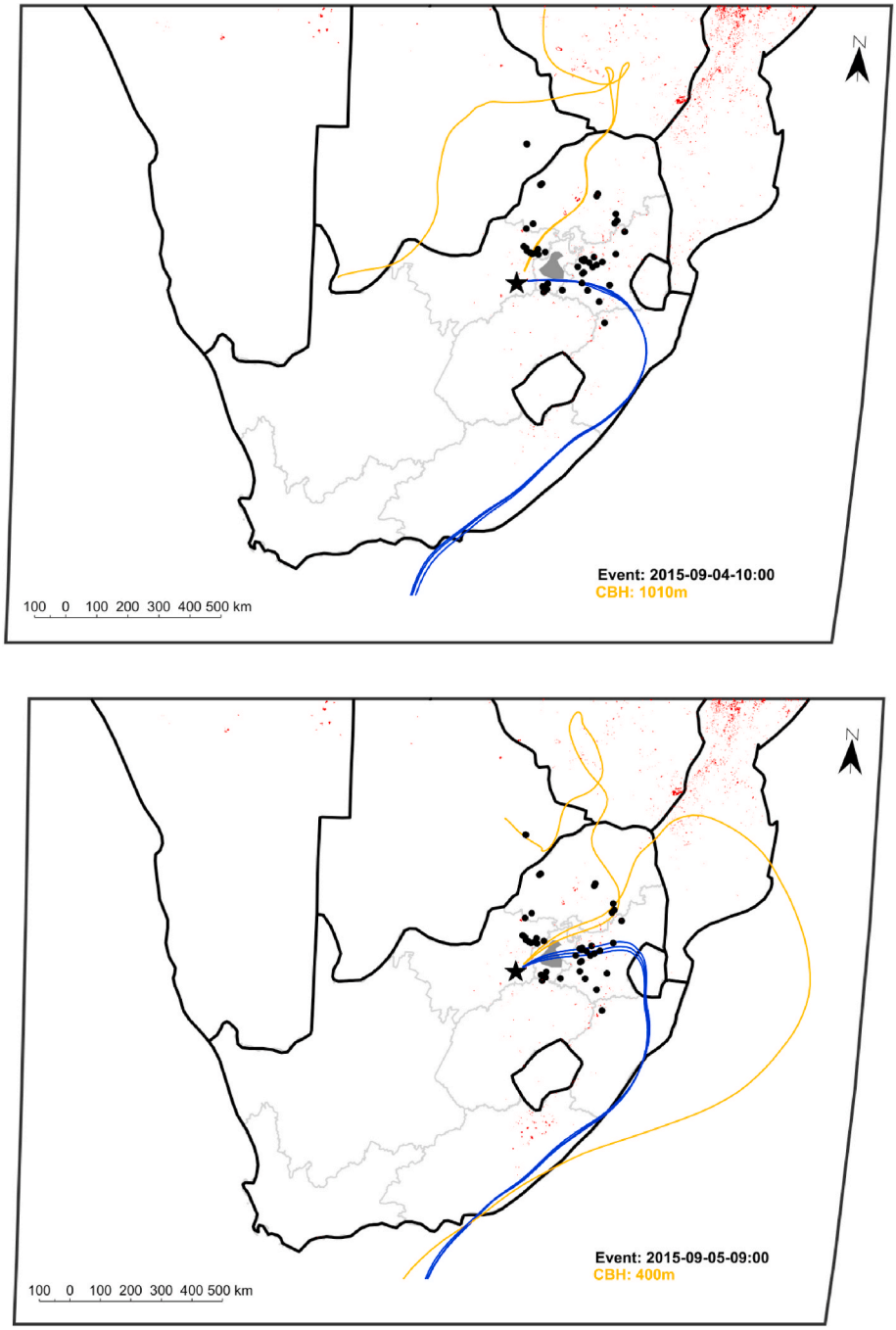

Fig. A6. Back trajectories at CBH and 100 m a.g.l. for rain events on 4 September 2015 (top) and 5 September 2015 (bottom), indicating below-cloud scavenging of pollutants.

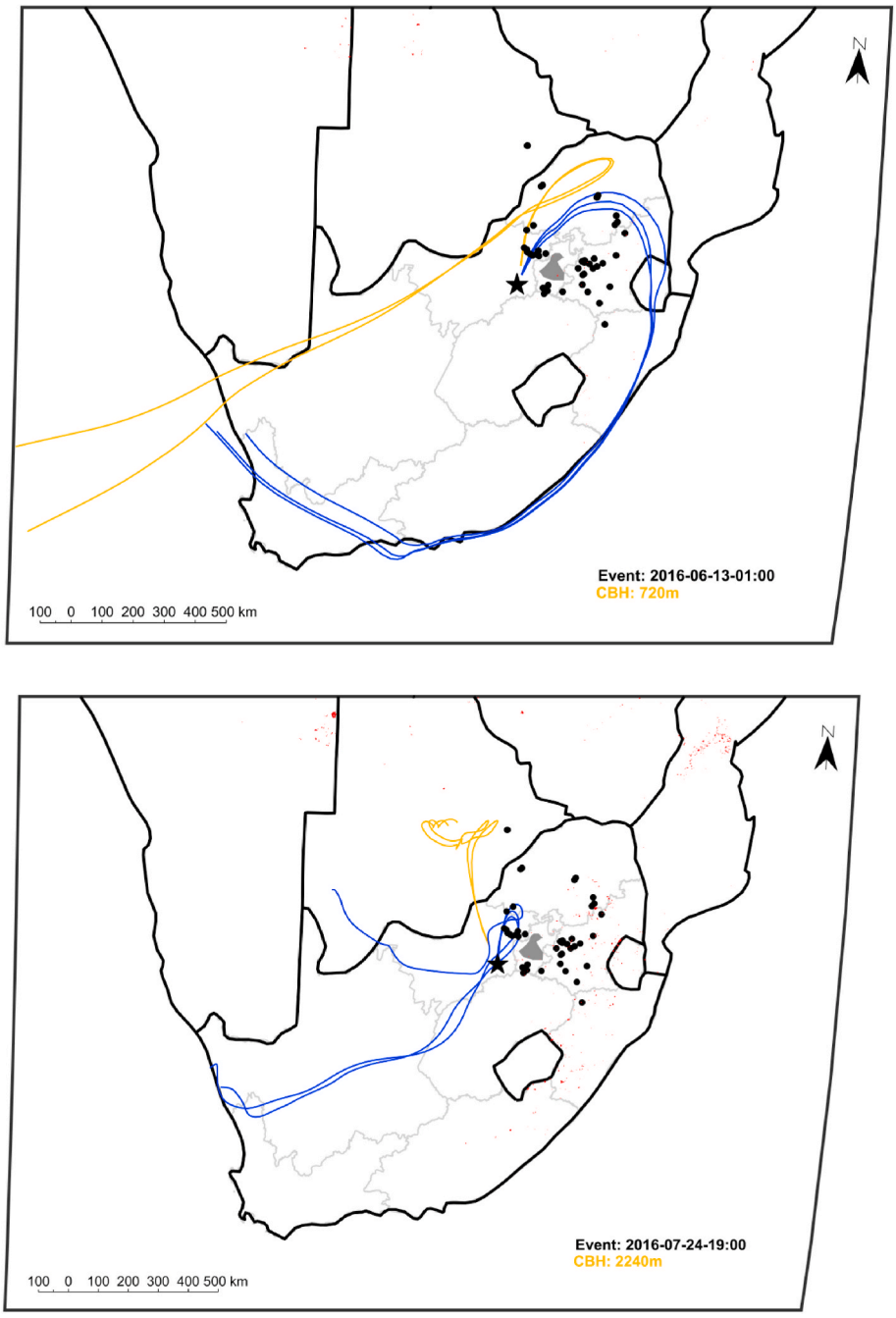

Fig. A7. Back trajectories at CBH and 100 m a.g.l. for rain events occurring in the South African winter on 13 June 2016 (top) and 24 July 2016 (bottom).

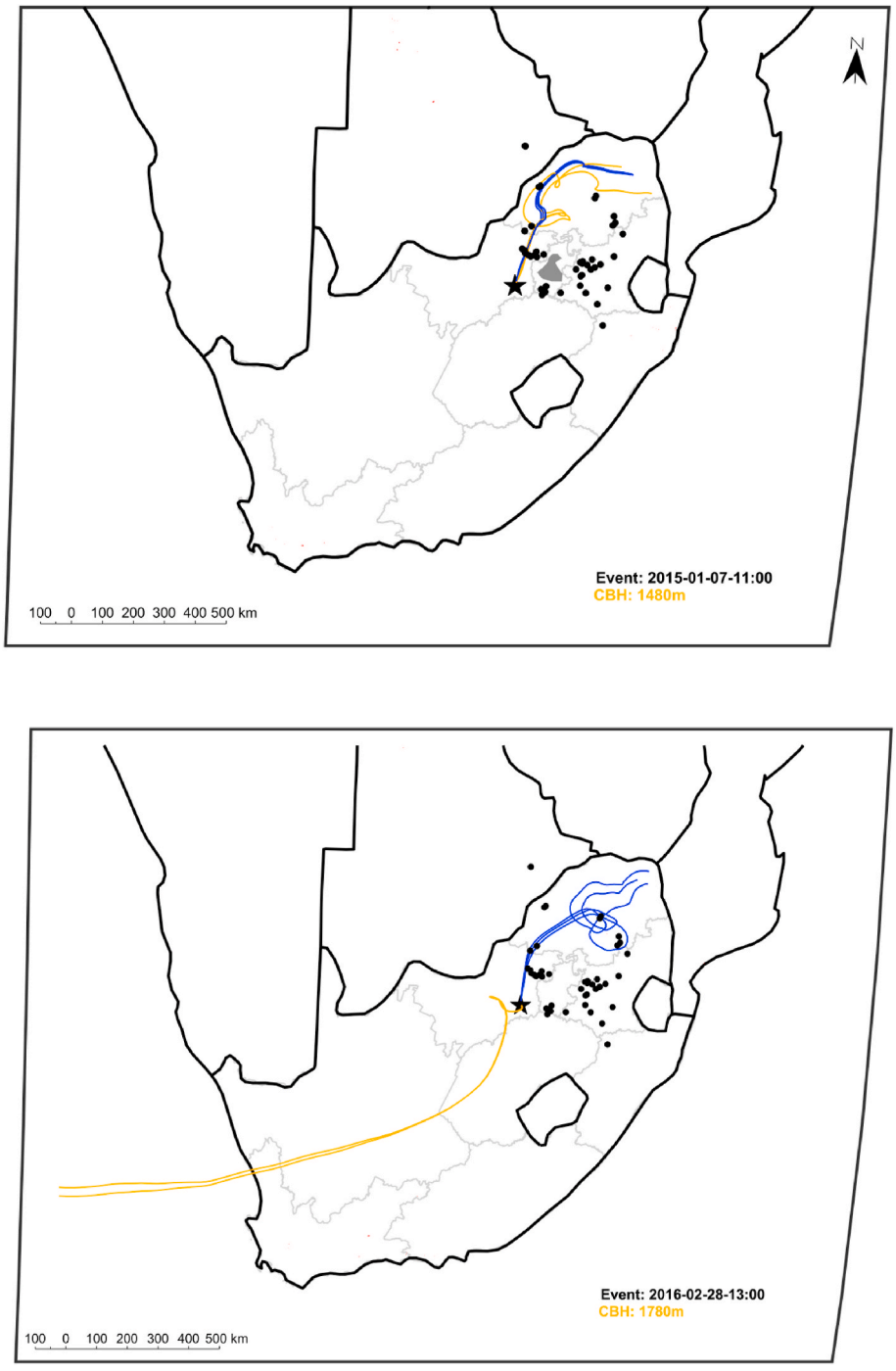

Fig. A8(a). Back trajectories at CBH and 100 m a.g.l. for rain events with the highest maximum (top) and highest average (bottom) rainfall intensities.

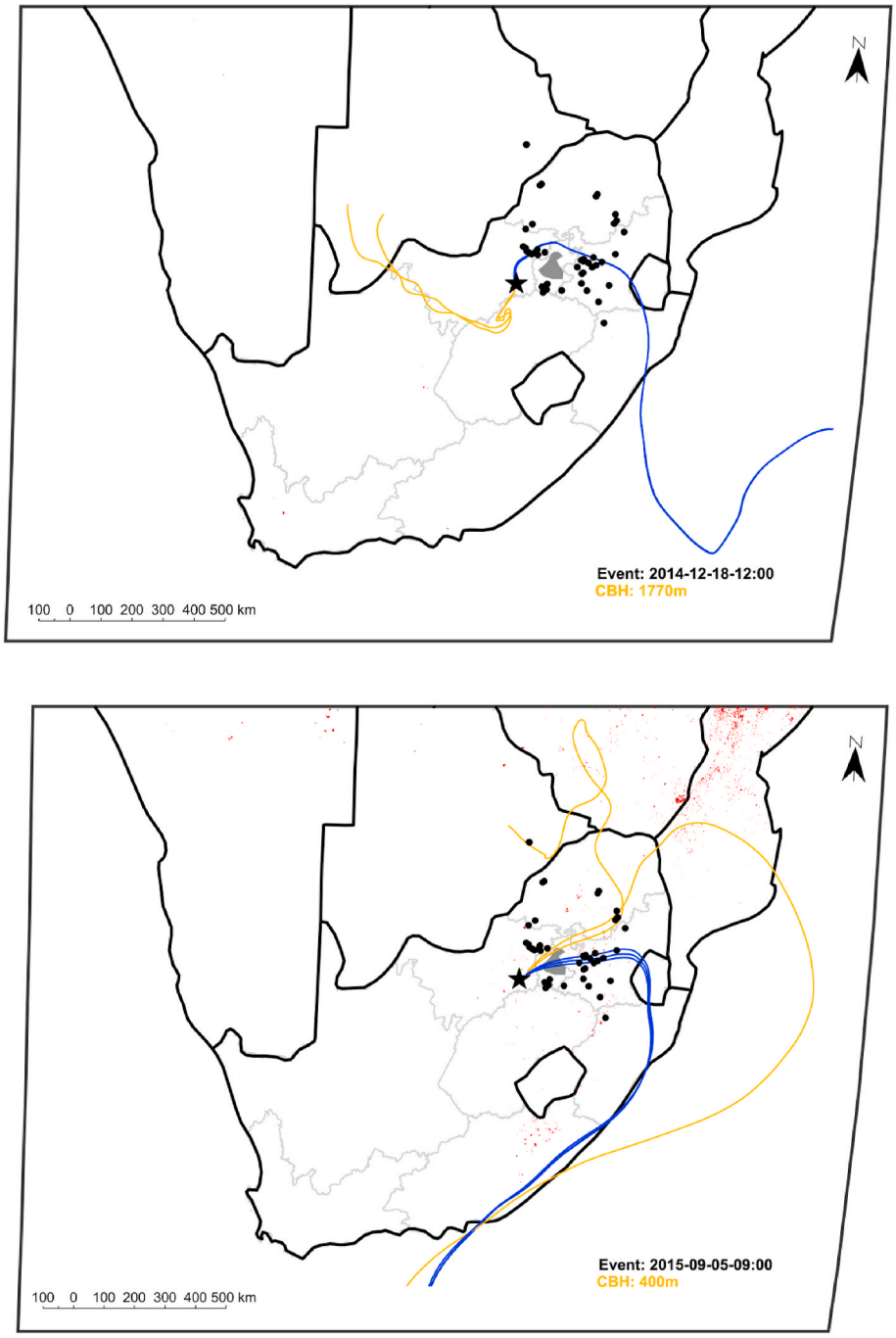

Fig. A8(b). Back trajectories at CBH and 100 m a.g.l. for two rain events with the lowest average rainfall intensities.

Table A1
Analyses of variance of ancillary measurements in the three cluster solutions based on ionic composition of rain

Variable	p-Value	Effect Sizes		
		A with B	A with C	B with C
pH	0.000	0.37	0.60	0.71
EC	0.001	0.53	0.81	0.07
SO_2	0.016	0.39	0.58	0.26
eBC	0.084	0.34	0.49	0.14
Intensity Max	0.000	0.45	1.12	0.81
Intensity Avg	0.084	0.27	0.75	0.42

References

Al-Khashman, O.A., 2009. Chemical characteristic of rainwater collected at a western site of Jordan. Atmos. Res. 91, 53–61.

Beukes, J.P., Venter, A.D., Josipovic, M., Van Zyl, P.G., Vakkari, V., Jaars, K., Dunn, M., Laakso, L., 2015. Chapter 6: automated continuous air monitoring. In: Forbes, P. (Ed.), Comprehensive Analytical Chemistry: Monitoring of Air Pollutants – Samling, Sample, Preparation and Analytical Techniques. Elsevier, Kidlington, Oxford, UK, Waltham, MA, USA.

Booyens, W., Van Zyl, P.G., Beukes, J.P., Ruiz-Jimenez, J., Kopperi, M., Riekkola, M.L., Josipovic, M., Venter, A.D., Jaars, K., Laakso, L., Vakkari, V., Kulmala, M., Pienaar, J.J., 2015. Size-resolved characterisation of organic compounds in atmospheric aerosols collected at Welgegund, South Africa. J. Atmos. Chem. 72, 43–64.

Brimblecombe, P., 2003. Aqueous phase chemistry of the troposphere. In: HEWITT, C.N., JACKSON, A. (Eds.), Handbook of Atmospheric Science: Principles and Applications. Blackwell Science, Oxford.

Chiloane, K.E., Beukes, J.P., Van Zyl, P.G., Maritz, P., Vakkari, V., Josipovic, M., Venter, A.D., Jaars, K., Tiitta, P., Kulmala, M., Wiedensohler, A., Liousse, C., Mkhatshw, G.V., Ramandh, A., Laakso, L., 2017. Spatial, temporal and source contribution assessments of black carbon over the northern interior of South Africa. Atmos. Chem. Phys. 17, 6177–6196.

Christner, B.C., Cai, R., Morris, C.E., Mccarter, K.S., Foreman, C.M., Skidmore, M.L., Montross, S.N., Sands, D.C., 2008. Geographic, seasonal, and precipitation chemistry influence on the abundance and activity of biological ice nucleators in rain and snow. Proc. Natl. Acad. Sci. USA 105, 18854–18859.

CIESIN, 2010. Columbia University, United Nations Food and Agriculture Programme (FAO), and Centro Internacional de Agricultura Tropical (CIAT), 2005, Gridded Population of the World: Future Estimates (GPWFE). Center for International Earth Science Information Network CIESIN. Palisades, NY: Socioeconomic Data and Applications Center (SEDAC). Columbia University.

Cohen, J., 1988. Statistical Power Analysis for the Behavioral Sciences. Routledge Academic, New York, NY.

Conradie, E.H., Van Zyl, P.G., Pienaar, J.J., Beukes, J.P., Galy-Lacaux, C., Venter, A.D., Mkhatshw, G.V., 2016. The chemical composition and fluxes of atmospheric wet deposition at four sites in South Africa. Atmos. Environ. 146, 113–131.

Costa-Surós, M., Calbó, J., González, J.A., Martin-Vide, J., 2013. Behavior of cloud base height from ceilometer measurements. Atmos. Res. 127, 64–76.

Ellis, S.M., Steyn, H.S., 2003. Practical significance (effect sizes) versus or in combination with statistical significance (p-values). Manag. Dynam.: J. South. Afr. Inst. Manag. Sci. 12, 51–53.

Emeis, S., Schafer–, K., Munkel–, C., Friedl, R., Suppan, P., 2012. Evaluation of the interpretation of ceilometer data with RASS and radiosonde data. Boundary-Layer Meteorol. 143, 25–35.

EUMETSAT, 2019. Monitoring Weather and Climate from Space.

Fedkin, N.M., Li, C., Dickerson, R.R., Canty, T., Krotkov, N.A., 2019. Linking improvements in sulfur dioxide emissions to decreasing sulfate wet deposition by combining satellite and surface observations with trajectory analysis. Atmos. Environ. 199, 210–223.

Feltracco, M., Barbaro, E., Kirchgeorg, T., Spolaor, A., Turetta, C., Zangrando, R., Barbante, C., Gambaro, A., 2019. Free and combined L- and D-amino acids in Arctic aerosol. Chemosphere 220, 412–421.

Finlayson-Pitts, B.J., Pitts JNR, J.N., 2000. Chemistry of the Upper and Lower Atmosphere: Theory, Experiments and Applications. Academic Press, California.

Fleming, Z.L., Monks, P.S., Manning, A.J., 2012. Review: untangling the influence of air-mass history in interpreting observed atmospheric composition. Atmos. Res. 1–39.

Fuentes, J.D., Chamecki, M., Nascimento Dos Santos, R.M., Von Randow, C., Stoy, P.C., Katul, G., Fitzjarrald, D., Manzi, A., Gerken, T., Trowbridge, A., 2016. Linking meteorology, turbulence, and air chemistry in the Amazon rain forest. Bull. Am. Meteorol. Soc. 97, 2329–2342.

Galloway, J.N., Savoie, D.L., Keene, W.C., Prospero, J.M., 1993. The temporal and spatial variability of scavenging ratios for nss sulfate, nitrate, methanesulfonate and sodium in the atmosphere over the North Atlantic Ocean. Atmos. Environ. 27A, 235–250.

Galy-Lacaux, C., Laouali, D., Descroix, L., Gobron, N., Liousse, C., 2009. Long term precipitation chemistry and wet deposition in a remote dry savanna site in Africa (Niger). Atmos. Chem. Phys. 9, 1579–1595.

Gierens, R., Henriksson, S., Josipovic, M., Vakkari, V., Van Zyl, P.G., Beukes, J.P., Wood, C.R., O'Connor, E.J., 2019. Observing continental boundary-layer structure and evolution over the South African savannah using a ceilometer. Theor. Appl. Climatol. 136, 333–346.

González, C.M., Aristizábal, B.H., 2012. Acid rain and particulate matter dynamics in a mid-sized Andean city: Th effect of rain intensity on ion scavenging. Atmos. Environ. 60, 164–171.

Hall, B.D., 2003. Atmospheric removal processes. In: HEWITT, C.N., JACKSON, A. (Eds.), Handbook of Atmospheric Science: Principles and Applications. Blackwell Science, Oxford.

Halsall, C.J., 2003. Regional-scale pollution problems. In: HEWITT, C.N., JACKSON, A. (Eds.), Handbook of Atmospheric Science: Principles and Applications. Blackwell Science, Oxford.

Harrison, M.S.J., 1986. A Synoptic Climatology of South African Rainfall Variations. PhD, University of Witwatersrand.

!"count(.//sb:host[1]//child::*//sb:date)">Hart, N.C.G., Reason, C.J.C., Fauchereau, N., . Tropical-extratropical interactions over Southern Africa: three cases of heavy summer season rainfall. Mon. Weather Rev. 138, 2608–2623.

Hart, N.C., Reason, C.J., Fauchereau, N., 2013. Cloud bands over southern Africa: seasonality, contribution to rainfall variability and modulation by the MJO. Clim. Dynam. 41, 1199–1212.

Jaars, K., Van Zyl, P.G., Beukes, J.P., Hellén, H., Vakkari, V., Josipovic, M., Venter, A.D., Räsänen, M., Knoetze, L., Cilliers, D.P., Siebert, S.J., Kulmala, M., Rinne, J., Guenther, A., Laakso, L., Hakola, H., 2016. Measurements of biogenic volatile organic compounds at a grazed savannah-grassland-agriculture landscape in South Africa. Atmos. Chem. Phys. 16, 15665–15688.

Kaufman, Y.J., Ichoku, C., Giglio, L., Korontzi, S., Chu, D.A., Hao, W.M., Li, R.-R., Justice, C.O., 2003. Fire and smoke observed from the Earth Observing System MODIS instrument - products, validation, and operational use. Int. J. Rem. Sens. 24, 1765–1781.

Kok, L., Van Zyl, P.G., Beukes, J.P., Swartz, J.-S., Burger, R.P., Ellis, S., Josipovic, M., Vakkari, V., Laakso, L., Kulmala, M., 2021. Chemical composition of rain at a regional site on the South African Highveld. WaterSA 47 (3), 326–337. https://doi.org/10.17159/wsa/2021.v47.i3.11861.

Kulshrestha, U.C., Reddy, L.A.K., Satyanarayana, J., Kulshrestha, M.J., 2009. Real-time wet scavenging of major chemical constituents of aerosols and role of rain intensity in Indian region. Atmos. Environ. 43, 5123–5127.

Laakso, L., Vakkari, V., Virkkula, A., Laakso, H., Backman, J., Kulmala, M., Beukes, J.P., van Zyl, Tiitta, P., Josipovic, M., Pienaar, J.J., Chiloane, K., Gilardoni, S., Vignati, E., Wiedensohler, A., Tuch, T., Birmili, W., Piketh, S., Collett, K., Fourie, G.D., Komppula, M., Lihavainen, H., de Leeuw, G., Kerminen, V.-M., 2012. South African EUCAARI measurements: seasonal variation of trace gases and aerosol optical properties. Atmos. Chem. Phys. 12, 1847–1864.

Laban, T.L., Van Zyl, P.G., Beukes, J.P., Vakkari, V., Jaars, K., Borduas-Dedekind, N., Josipovic, M., Thompson, A.M., Kulmala, M., Laakso, L., 2018. Seasonal influences on surface ozone variability in continental South Africa and implications for air quality. Atmos. Chem. Phys. 18, 15491–15514.

Lakens, D., 2013. Calculating and reporting effect sizes to facilitate cumulative science: a practical primer for t-tests and ANOVAs. Front. Psychol. 4 (863), 1–12.

Laouali, D., Galy-Lacaux, C., Diop, B., Delon, C., Orange, D., Lacaux, J.P., Akpo, A., Lavenu, F., Gardrat, E., Castera, P., 2012. Long term monitoring of the chemical composition of precipitation and wet deposition fluxes over three Sahelian savannas. Atmos. Environ. 50, 314–327.

Lourens, A.S.M., Butler, T.M., Beukes, J.P., Van Zyl, P.G., Beirle, S., Wagner, T.K., Heue, K.-P., Pienaar, J.J., Fourie, G.D., Lawrence, M.G., 2012. Re-evaluating the NO2 hotspot over the South African Highveld. South Afr. J. Sci. 108 (9/10), 6. Art. #1146.

Lutgens, F.K., Tarbuck, E.J., 1982. The Atmosphere: an Introduction to Meteorology. Prentice-Hall, New Jersey.

Lynn, B.H., Khain, A.P., Dudhia, J., Rosenfeld, D., Pokrovsky, A., Seifert, A., 2005. Spectral (bin) microphysics coupled with a mesoscale model (MM5). Part II: simulation of a CaPE rain event with a squall line. Am. Meteorolog. Soc. 133, 59–71.

Meth, O., 2018. New Satellite Data Reveals the World's Largest Air Pollution Hotspot Is Mpumalanga- South Africa. Greenpeace.

Mogale, M., Dyson, L.L., 2017. Continental Tropical Low-Pressure Systems and Their Associated Rainfall over the Highveld of South Africa Using Self-Organizing Maps, pp. 62–65.

Mompati, M.K., Piketh, S.J., Aas, W., Van Zyl, P.G., Pienaar, J.J., Curtis, C.J., 2022. Rainwater chemistry and total deposition of acidity from the northern savanna to the southern coastal fynbos of South Africa. Water Air Soil Poll. 233 (275).

Mphepya, J.N., Pienaar, J.J., Galy-Lacaux, C., Held, G., Turner, C.R., 2004. Precipitation chemistry in semi-arid areas of southern Africa: a case study of a rural and an industrial site. J. Atmos. Chem. 47, 1–24.

Mphepya, J.N., Galy-Lacaux, C., Lacaux, J.P., Held, G., Pienaar, J.J., 2006. Precipitation chemistry and wet deposition in Kruger National Park, South Africa. J. Atmos. Chem. 53, 169–183.

Orué, M.R., Gaiero, D., Kirschbaum, A., 2019. Seasonal characteristics of the chemical composition of rainwaters from Salta city, NW Argentina. Environ. Earth Sci. 78.

Pauliquevis, T., Lara, L.L., Antunes, M.L., Artaxo, P., 2012. Aerosol and precipitation chemistry measurements in a remote site in Central Amazonia: the role of biogenic contribution. Atmos. Chem. Phys. 12, 4987–5015.

Preston-Whyte, R.A., Tyson, P.D., 1988. The Atmosphere and Weather of Southern Africa. Oxford University Press, Cape Town, SA.

SAWS, 2019b. Historical Rain. South African Weather Service.

SAWS, 2019. South African Weather Service (SAWS).

Schwab, J.J., Casson, P., Brandt, R., Husain, L., Dutkewicz, V., Wolfe, D., Demerjian, K.L., Civerolo, K.L., Rattigan, O.V., Felton, H.D., Dukett, J.E., 2016. Atmospheric chemistry measurements at Whiteface Mountain, NY: cloud water chemistry, precipitation chemistry, and particulate matter. Aerosol Air Qual. Res. 16, 841–854.

Seinfeld, J.H., Pandis, S.N., 2006. Atmospheric Chemistry and Physics: from Air Pollution to Climate Change, 2 ed. John Wiley & Sons, NJ.

Statsoft, I., 2006. SATISTICA (Data Analysis Software System), 7.1.

Stein, A.F., Draxler, R.R., Rolph, G.D., Stunder, B.J.B., Cohen, M.D., Ngan, F., 2015. NOAA's HYSPLIT Atmospheric Transport and Dispersion Modeling System. American Meteorological Society, pp. 2059–2077.

Stern, D.I., 2006. Reversal of the trend in global anthropogenic sulfur emissions. Global Environ. Change 16, 207–220.

Stohl, A., Eckhardt, S., Forster, C., James, P., Spichtinger, N., Seibert, P., 2002. A replacement for simple back trajectory calculations in the interpretation of atmospheric trace substance measurements. Atmos. Environ. 36, 4635–4648.

Sun, M., Wang, Y., Wang, T., Fan, S., Wang, W., Li, P., Guo, J., Li, Y., 2010. Cloud and the corresponding precipitation chemistry in south China: water-soluble components and pollution transport. J. Geophys. Res. 115, D22303.

Tosen, G.R., Jury, M., 1988. Climatology of the winter boundary layer over the eastern Transvaal. S. Afr. J. Sci. 84 (4), 247.
Tost, H., Jöckel, P., Kerkweg, A., Pozzer, A., Sander, R., Lelieveld, J., 2007. Global cloud and precipitation chemistry and wet deposition: tropospheric model simulations with ECHAM5/MESSy1. Atmos. Chem. Phys. 7, 2733–2757.
Tyson, P.D., Preston-Whyte, R.A., 2017. The Weather and Climate of Southern Africa. Oxford University Press, Cape Town, South Africa.
Tyson, P.D., Preston-Whyte, R.A., Diab, R.D., 1976. Towards an inversion climatology of southern Africa: Part I, surface inversions. S. Afr. Geogr. J. 58 (2), 151–163. https://doi.org/10.1080/03736245.1976.10559577.
Uchiyama, R., Okochi, H., Ogata, H., Katsumi, N., Nakano, T., 2019. Characteristics of trace metal concentration and stable isotopic composition of hydrogen and oxygen in "urban-induced heavy rainfall" in downtown Tokyo, Japan; the implication of mineral/dust particles on the formation of summer heavy rainfall. Atmos. Res. 217, 73–80.
VAISALA, 1999. In: VAISALA (Ed.), Ceilometer CT25K User's Guide.
Venter, A.D., Van Zyl, P.G., Beukes, J.P., Josipovic, M., Hendriks, J., Vakkari, V., Laakso, L., 2017. Atmospheric trace metals measured at a regional background site (Welgegund) in South Africa. Atmos. Chem. Phys. 17, 4251–4263.
Venter, A.D., Van Zyl, P.G., Beukes, J.P., Josipovic, M., Jaars, K., Booyens, W., Vakkari, V., Laakso, L., Kulmala, M., 2018. Size-resolved characteristics of inorganic ionic species in atmospheric aerosols at a regional background site on the South African Highveld. J. Atmos. Chem. 75 (3), 285–304.
Wallace, J.M., Hobbs, P.V., 2006. Cloud microphysics. In: DMOWSKA, R., HARTMANN, D., ROSSBY, H.T. (Eds.), Atmospheric Science: an Introductory Survey. Canada. Elsevier.
WMO, 2004. In: WATCH, W.M.O.G.A. (Ed.), Manual for the GAW Precipitation Chemistry Programme.
Xu, D., Ge, B., Wang, Z., Sun, Y., Chen, Y., Ji, D., Yang, T., Ma, Z., Cheng, N., Hao, J., 2017. Below-cloud wet scavenging of soluble inorganic ions by rain in Beijing during the summer of 2014. Environ. Pollut. 230, 963–973.
Yao, Z.T., Ji, X.S., Sarker, P.K., Tang, J.H., Ge, L.Q., Xia, M.S., XI, Y.Q., 2015. A comprehensive review on the applications of coal fly ash. Earth Sci. Rev. 141, 105–121.
Zhang, Y., Kang, S., Li, C., Cong, Z., Zhang, Q., 2012. Wet deposition of precipitation chemistry during 2005-2009 at a remote site (Nam Co Station) in central Tibetan Plateau. J. Atmos. Chem. 69, 187–200.
Zhao, S., Yu, Y., He, J., Yin, D., Wang, B., 2015. Below-cloud scavenging of aerosol particles by precipitation in a typical valley city, northwestern China. Atmos. Environ. 102, 70–78.